Äspö Hard Rock Laboratory

Prototype Repository

Acoustic emission and ultrasonic monitoring results from deposition hole DA3545G01 in the Prototype Repository between April 2007 and September 2007

F. Zolezzi

J.R. Haycox

W.S. Pettitt

Applied Seismology Consultants

November 2008

SKB

Äspö Hard Rock Laboratory

Äspö Hard Rock Laboratory

Prototype Repository

Acoustic emission and ultrasonic monitoring results from deposition hole DA3545G01 in the Prototype Repository between April 2007 and September 2007

F. Zolezzi

J.R. Haycox

W.S. Pettitt

Applied Seismology Consultants

November 2008

Report DLV-08-06

To

SKB

APPLIED SEISMOLOGY CONSULTANTS

Last Edited	4 November 2008
File name	SKBProto_Apr07Sep07_04112008.doc
Last Printed	04 November 2008
Signature	

Executive summary

This report describes results from acoustic emission (AE) and ultrasonic monitoring around a canister deposition hole (DA3545G01) in the Prototype Repository Experiment at SKB's Hard Rock Laboratory (HRL), Sweden. The experiment has been designed to simulate a disposal tunnel in a real deep repository for removal of high-level radioactive waste.

The test consists of a 90m long, 5m diameter sub-horizontal tunnel excavated in dioritic granite. The monitoring aims to examine changes in the rock mass caused by an experimental repository environment, in particular due to thermal stresses induced from canister heating and pore pressures induced from tunnel sealing.

Two techniques are utilised here to investigate the processes occurring within the rock mass around the deposition hole: ultrasonic survey and acoustic emission (AE). Ultrasonic surveys are used to 'actively' examine the rock. Velocity changes are measured between transmitter-receiver pairs using a cross-correlation technique that allows a velocity resolution of ± 2 m.s^{-1}. Amplitude and velocity changes on the ray paths can then be interpreted in terms of changes in the material properties of the rock. Calculations using the velocities can determine the changes in dynamic moduli, Young's modulus and Poisson's ratio, to give direct indications of the properties of the rock through which the ray paths travel. Crack density and saturation can also be calculated to determine changes in crack properties in the damaged and disturbed zones. AE monitoring is a 'passive' technique similar to earthquake monitoring but on a much smaller distance scale (source dimensions of millimetres). AEs occur on fractures in the rock when they are created or when they move.

This report relates to the period between 1st April 2007 and 30th September 2007, and is the fifth of a 6-monthly processing and interpretation of the results for the heating and pressurisation phase of the experiment. Ultrasonic monitoring has been conducted at the Prototype Repository since September 1999. During excavation, monitoring of both deposition holes in section 2 of the Prototype Tunnel was undertaken to delineate zones of stress related fracturing and quantitatively measure fracturing in the damaged zone. A permanent ultrasonic array was installed in the rock mass in June 2002 around deposition hole DA3545G01.

During this monitoring period, we observed a general increase in velocity and amplitude for both P- and S-wave arrivals in all the ray-paths analysed. P- and S-wave velocity increases between 20th and 26th April 2007 by an average of 0.5 m.s^{-1}. This increase can be related to the increase in pressure in the backfill over the deposition hole. The magnitude of the average changes is less than the velocity resolution of 2 m.s^{-1} estimated for ultrasonic measurements but changes on individual ray paths are significant. Average velocity changes are also observed on 6th May 2007 and 25th June 2007.

Amplitudes also exhibit an increase between the 20th and 26th April. The increase for P-waves is 1.0 dB, while S-waves increase by 0.3 dB. As for velocity change, this can be related to the increase in pressure in the backfill over the deposition hole. For the remaining five months, the amplitudes exhibit a constant increase. P-waves increase to a greater extent, ending the monitoring period 1.5 dB greater than at the start. S-waves increase by 0.6 dB over this time.

Ray paths have been categorised following spatial criteria presented in previous reporting periods. For all ray path categories examined the variations observed for both P- and S-wave amplitudes and velocities are very similar, showing the same increment during April 2007. The higher changes, both in amplitudes and velocities, are observed in category 'Far'. Changes in Young's Modulus, Poisson's Ratio, Crack Density and Saturation Parameters have been calculated from the average measured velocities for different ray path categories.
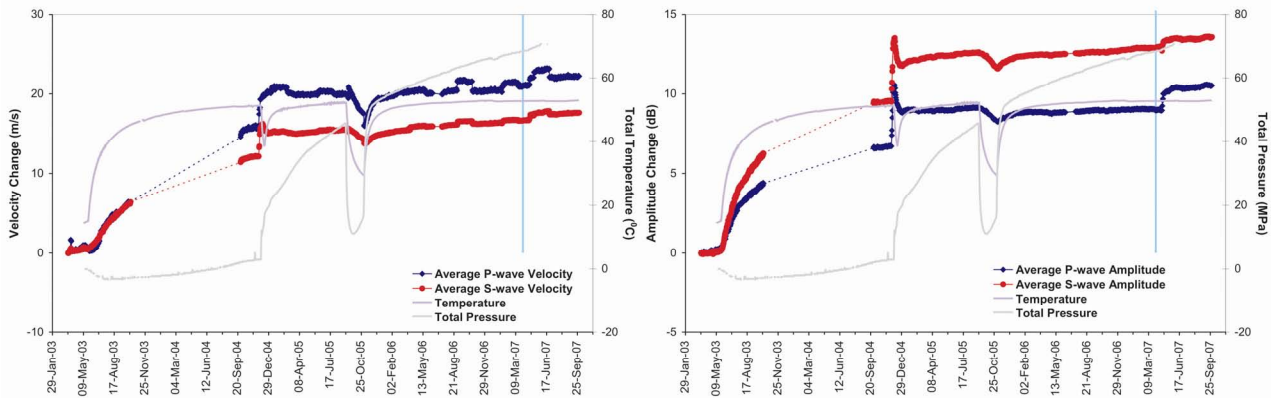

Average velocity change and amplitude change since the start of heating and pressurisation at the Prototype repository. The blue line shows the start of the period analysed in this report (Apr. 07 –Sept. 07).

Young's Modulus and Saturation increase at the end of April and then decrease at the end of June 2007 showing the same trend as P- and S-wave velocities. Poisson's ratio shows less variation in its values. Crack density shows the opposite behaviour displaying a decrease on the end of April, followed by an increase on the end of June 2007. All the ray paths follow the same trend but the category that shows highest variation is 'Far'. These changes can be related with the rapid changes in pressure in the backfill over deposition hole DA3545G01.

During this six-month period we triggered 221 events and located 115 AEs. The rate of triggers remains reasonably constant. We have an average of 1.21 triggers recorded per day. The maximum triggered events recorded are on 25th April 2006 (6 events). An average of 2 events is located per day with a maximum of 4 located AEs on 30th September 2007.

A study of the spatial distribution of AEs shows that all the events are located in 3 tight clusters that we define A, B and C (see the following figure). Events in the individual clusters are located close enough together to be considered occurring on the same feature and occur over the whole reporting period with no significant peaks in activity. Cluster A is made of 54 events located in the south-east side of deposition hole DA3545G01, while cluster B (47 events) and cluster C (14 events) are on south-west of deposition hole DA3545G01. Clusters A and B were recognized in the previous six-months reporting period. Cluster C has not been identified previously but is located in the region of activity which occurred during excavation. The first cluster (A) locates in a region of low-compressive or tensile stresses. The other clusters (B and C) are located in a region of high compressive stresses. AEs may be occurring at these positions due to the presence of pre-existing microcracks, generated during excavation. The AEs are characterized by relatively low magnitudes with respect to previous periods, which means that the clusters do not represent significant activity.

6

Although some changes in measured velocities, signal amplitudes and acoustic emission activity have been observed, the rock mass has remained relatively stable. This is consistent with a relatively stable period of environmental characteristics (temperature and pressure).
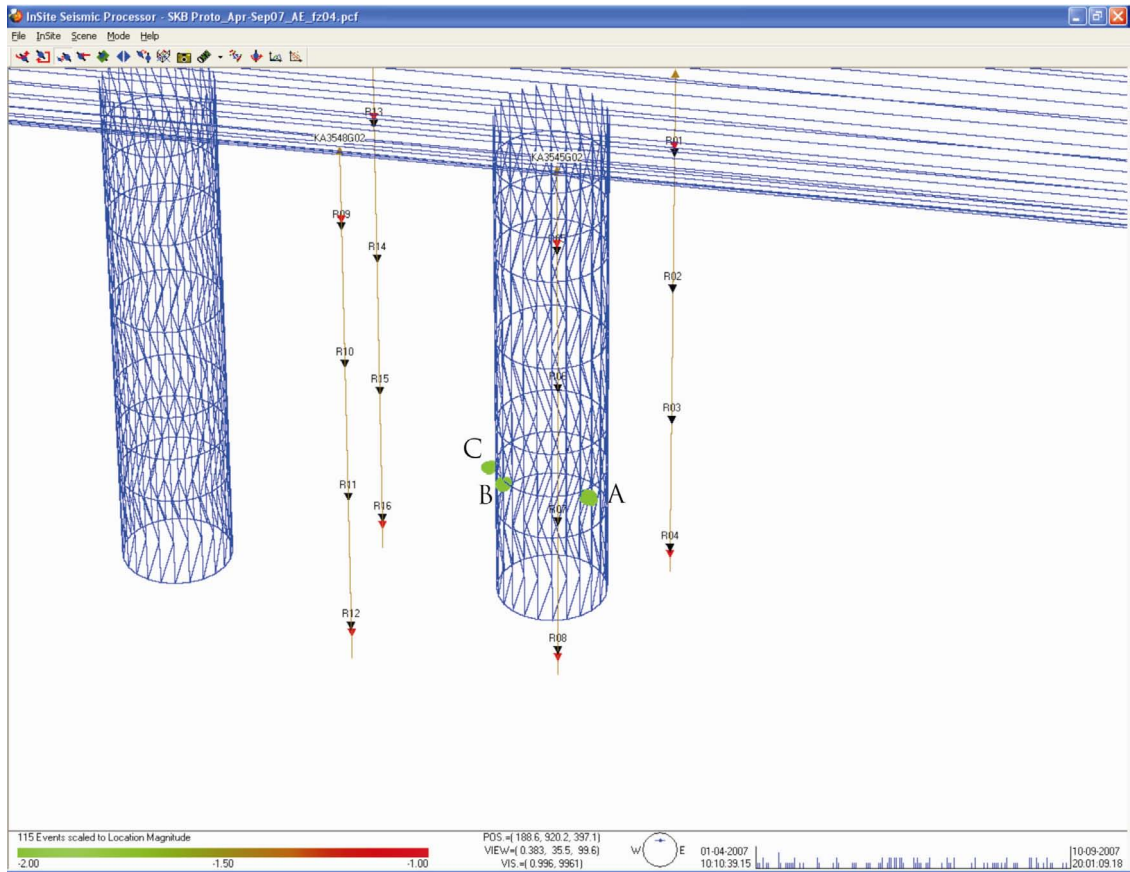
Clusters (defined 'A', 'B' and 'C') of AE activity observed on the South side of deposition hole DA3545G01.

Sammanfattning

Denna rapport beskriver resultaten från AE-mätningar och ultaljudsmätningar runt deponeringshål DA3545G01 i prototypförvaret vid SKB:s Hard Rock Laboratory. Experimentet har designats för att simulera en deponeringstunnel i ett verkligt djupförvar för högaktivt radioaktivt avfall.

Försöket består av en 90 m lång horisontell tunnel med en diameter på 5 m, uttagen ur en dioritisk granit. Syftet med mätningen är att undersöka förändringar i bergmassan som orsakats av en experimentell förvarsmiljö, speciellt med avseende på värmespänning från uppvärmning av kapseln och portryck orsakade av förseglingen av tunneln.

Två tekniker används för att undersöka de processer som förekommer i bergmassan runt deponeringshålet; ultraljudsmätning och AE-övervakning. Ultraljudsmätning används för att "aktivt" undersöka berget. Hastighetsförändringar mäts mellan sändare - givare genom att använda en kors-korrelationsteknik som möjliggör en mätnoggrannhet på ± 2 m.s^{-1}. Förändringar i amplitud och hastighet hos signalen när den passerat genom bergmassan i olika signalvägar relativt deponeringshålen, ("ray path") har sedan använts för att undersöka förändringar i bergegenskaperna. Hastigheterna användas för att bestämma förändringar i dynamisk modul, elasticitetsmodul och tvärkontraktionstal som ger direkta indikationer på egenskaperna på berget genom vilket vägen passerar. Sprickdensitet och vattenmättnadsgrad kan också beräknas för att fastställa förändringar i sprickornas egenskaper i den skadade och störda zonen. AE-övervakning är en 'passiv' teknik som liknar jordbävningsövervakning men på en mycket mindre avståndsskala (dimensioner på källan i millimetrar). AE (Acoustic Emission) uppkommer hos bergssprickor när de bildas eller när de rör sig

Denna rapport behandlar mätningar under perioden 1:a april 2007 till 30:e september 2007 och är den femte rapporten med processning och tolkning av data från testerna. Ultraljudsmätningar har utförts i projektet Prototype Repository sedan september 1999. Mätningar gjordes runt de båda deponeringshålen i sektion 2 under borrningen av hålen. Syftet med dessa mätningar var att beskriva zoner med spänningsrelaterade sprickor och kvantitativt mäta sprickutbildningen i den störda zonen runt deponeringshålen. Ett permanent ultraljudssystem installerades i berget runt deponeringshål DA3545G01 i juni 2002.

Under denna mätperiod observerade vi en generell ökning i hastighet och amplitud för både P- och S-vågen. Detta gäller för samtliga undersökta signalvägar (ray path). P- och S-vågornas hastighet ökade mellan den 20:e och 26:e april 2007 i medeltal med 0.5 1 m.s^{-1}. Denna ökning kan relateras till ökningen av trycket i återfyllningen över deponeringshålet. Magnituden på förändringen i medeltal är mindre än mätnoggrannheten på 2 m.s^{-1} uppskattade för ultraljudsmätningar men ändringarna för individuella signalvägar är signifikanta. Förändringar i medelhastigheten observerades också den 6:e maj 2007 och den 25:e juni 2007.

Amplituden uppvisade också en ökning mellan den 20:e och 26:e april. Ökningen för P-vågorna är 1.0 dB medan S-vågorna ökar med 0.3 dB. Precis som för hastighetsändringen kan detta relateras till ökningen av trycket i återfyllningen över deponeringshålet. Under de återstående 5 månaderna uppvisade amplituden en konstant ökning. P-vågorna ökar mest och vid slutet av mätperioden är den 1.5 dB högre än vid starten. S-vågorna ökar med 0.6 dB under motsvarande tidsperiod.

De olika signalvägarna relativt deponeringshålen ("ray path") har kategoriserats enligt rumsliga kriterier som pressenterats i tidigare rapporteringar. Både P och S-vågorna observerade variationer i amplituder och hastigheter är likartade för alla undersökta signalvägar. De större förändringarna i amplitud och hastighet observeras för kategorin "Far". Förändringar i E-modul, tvärkontraktionstal, sprickdensitet och vattenmättnadsgrad har beräknats med hjälp av medelhastigheter för olika kategorier av signalvägar. E-modul och vattenmättnadsgrad ökar under slutet av april och minskar sedan i slutet av juni 2007 d.v.s. de följer samma trend som P- och S-vågornas hastigheter. Tvärkontraktionstalet uppvisar mindre variation. Sprickdensiteten uppvisar den motsatta trenden d.v.s. en minskning i slutet av april följt av en ökning i slutet av juni 2007. Alla signalvägar uppvisar samma trend men den kategorin som uppvisar den högsta variationen är "Far". Förändringarna kan relateras till den snabba ändringen i tryck i återfyllningen över deponeringshålet DA3545G01.
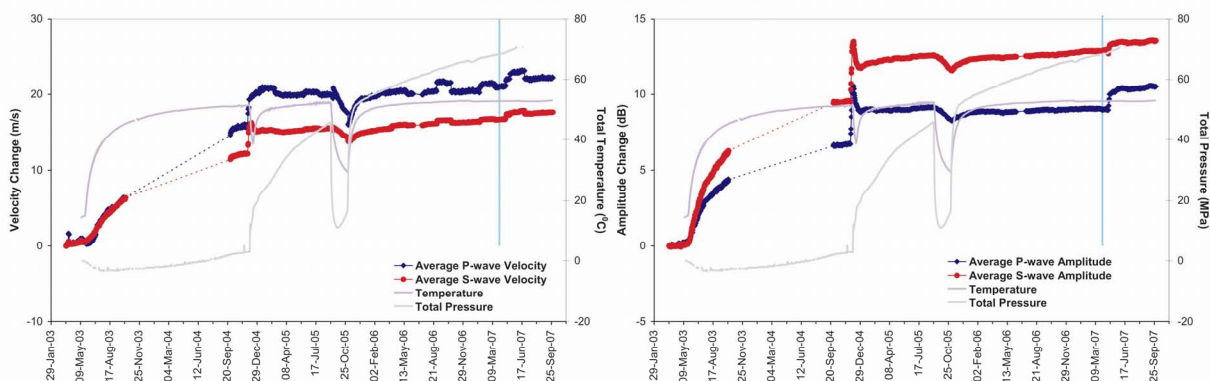
Medelhastighets- och amplitudförändring. Den vertikala blå linjen anger starten på perioden som analyseras i denna rapport (april 2007 - september 2007).

Under denna sexmånadsperiod utlöstes 221 händelser och lokaliserade115 AE:s (**A**coustic **E**mission). Takten på utlösta händelser är relativt konstant, i medeltal 1.21 händelser per dag. Maximala antalet utlösta händelser observerades den 25:e april 2007 (6 händelser). I medeltal lokaliserades 0.63 händelser per dag med ett maximum av 4 st den 30:e september 2007.

Studie av den rumsliga fördelningen av AE visar att alla händelser är lokaliserade till 3 täta kluster som vi definierar A, B och C (se figur nedan). Händelserna i det enskilda klustret är lokaliserade så nära varandra att de kan anses ha uppkommit på samma anomali och uppträder under hela mätperioden utan någon signifikant aktivitetsmaximum. Kluster A består av 54 händelser lokaliserade till sydöstra sidan av deponeringshålet DA3545G01 medan kluster B (46 händelser) och kluster C (14 händelser) ligger på sydvästra sidan av deponeringshålet DA3545G01. Kluster A och B syntes under den föregående 6-månadersperideon. Kluster C har inte blivit identifierad

tidigare men den är lokaliserad till regionen med aktiviteter som uppstod under uttaget för deponeringshålet. Kluster A ligger i regioner med låga tryckspänningar eller med dragspänningar. De andra klustren (B och C) ligger i regioner med höga kompressionsspänningar. AE kan uppstå i dessa positioner på grund av närvaro av mikrosprickor som uppstod under uttaget av deponeringshålet. De registrerade AE karakteriseras av relativt låga magnituder i förhållande till tidigare perioder vilket betyder att klustren inte representerar signifikant aktivitet.

Trots att vissa förändringar i uppmätta hastigheter, signalamplitud och akustiska aktivitere har observerats så förblir bergmassan relativt stabil. Detta är förenligt med en relativt stabil period vad gäller tryck och temperatur i bergmassan.
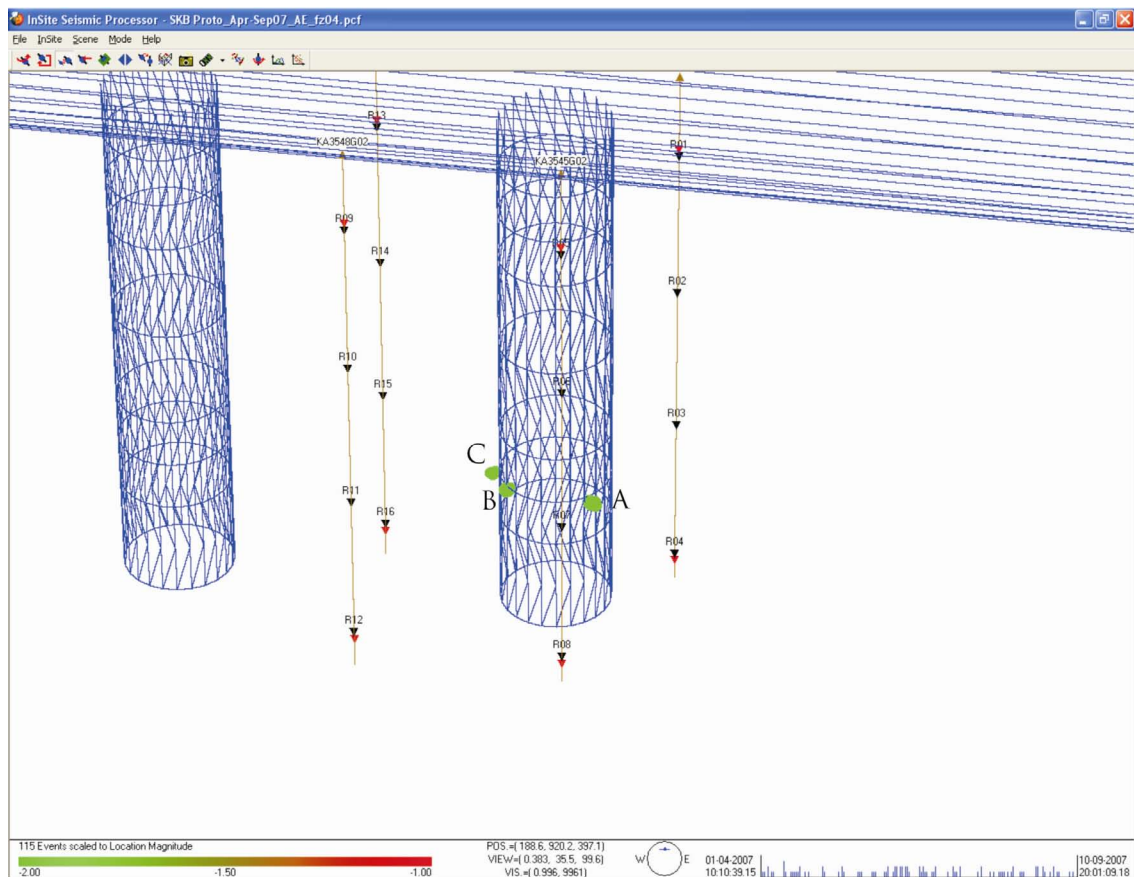
Kluster A, B och C av AE-aktiviteter observerade på södra väggen av deponeringshål DA3545G01.

Contents

Table of Figures

Table of Tables

1 Introduction

This report describes results from acoustic emission (AE) and ultrasonic monitoring around a canister deposition hole (DA3545G01) in the Prototype Repository Experiment at SKB's Hard Rock Laboratory (HRL), Sweden. The monitoring aims to examine changes in the rock mass caused by an experimental repository environment,
in particular due to thermal stresses induced from canister heating and pore pressures induced from tunnel sealing. Monitoring of this volume has previously been performed during excavation [*Pettitt et al.*, 1999], and during stages of canister heating and tunnel pressurisation [*Haycox et al.,* 2005a,b; *Haycox et al.*, 2006a,b, *Zolezzi et al.*, 2007]. Further information on this monitoring can be found in Appendix I. This report relates to the period between 1st April 2007 and 30th September 2007, and is the fifth of a
6-monthly processing and interpretation of the results for the experiment.

The Prototype Repository Experiment (Figure 1-1) has been designed to simulate a disposal tunnel in a real deep repository for disposal of high-level radioactive waste. Its objective is 'to test and demonstrate the integrated function of the repository components under realistic conditions on a full scale and to compare results with models and assumptions'. The experiment consists of a 90m long, 5m diameter sub-horizontal tunnel excavated in a dioritic granite using a Tunnel Boring Machine (TBM). The rock mass has two main discontinuous sets of sparse, en-echelon fractures [*Patel et al.*, 1997]. The Prototype Repository design incorporates six full-scale canister deposition holes which have been excavated vertically into the floor of the tunnel using a TBM converted to vertical boring. Each deposition hole measures 1.75m in diameter and approximately 8.8m in length. Simulated waste canisters, encased in a bentonite buffer, have been placed into each deposition hole and heated from within by specially designed electric heaters to simulate disposed radioactive material at elevated temperatures. The tunnel was then backfilled using a mixture of bentonite and crushed rock, and sealed using concrete plugs. A range of measurements are made in and around the tunnel and deposition holes.
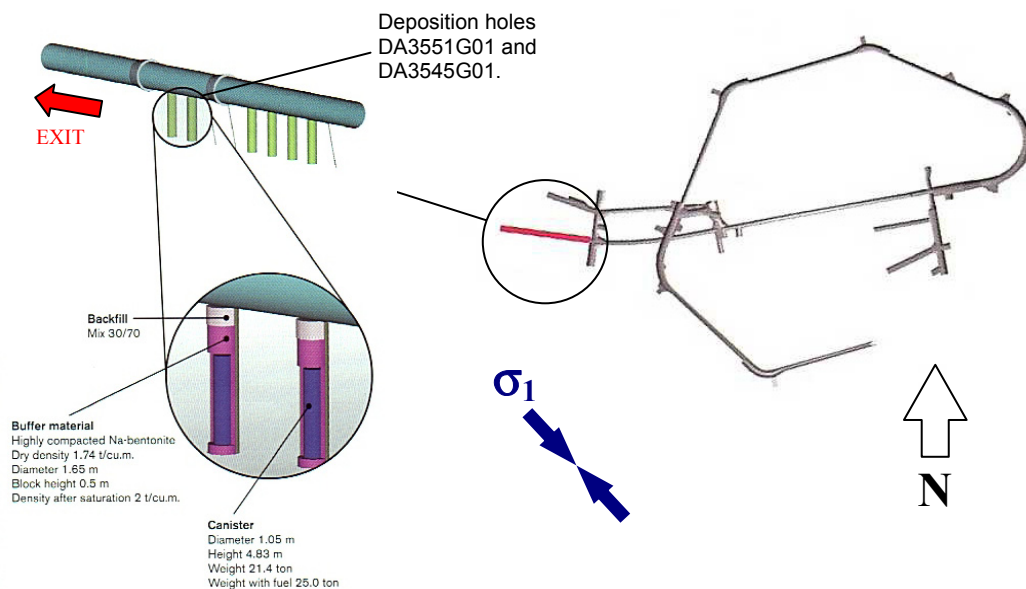
Figure 1-1: *Plan view of the experimental tunnels at the Äspö HRL and the location of the Prototype Repository. A schematic illustration of the final experimental set up is shown with canisters and bentonite clay buffer installed in the 1.75m diameter deposition holes. Note the entrance of the tunnel is towards the left. Graphics are modified from SKB[1999].*

AE and ultrasonic monitoring is a tool for remotely examining the extent and severity of damage and disturbance around an excavation. This can be induced by the excavation method itself; by the redistribution of stresses (loading or unloading) resulting from the void or by environmental effects such as heating, saturation or pressurisation. Acoustic techniques are particularly adept at assessing the Excavation Damaged or Disturbed Zone (EDZ) as they allow it to be mapped spatially and temporally with high resolution, and they allow the effect on the rock mass to be quantifiably measured. Furthermore, acoustic techniques allow investigations to be conducted remotely, without the need for potentially damaging coring. *Young and Pettitt*[2000] give a review of AE and ultrasonic results from a number of experiments conducted in different underground environments.

- AE monitoring is a 'passive' technique similar to earthquake monitoring but on a much smaller distance scale (source dimensions of millimetres). AEs occur on fractures in the rock sample when they are created or when they move. The data acquisition system triggers on AEs when they occur and records full-waveform information that can then be used to delineate the amount, time, location and mechanism of fracturing.

- Ultrasonic surveys are used to 'actively' examine the rock. In this case an array of transmitters sends signals to an array of receivers. Amplitude and velocity changes on the ray paths can be interpreted in terms of changes in the material properties of the rock. Calculations using the velocities can determine changes in dynamic moduli, Young's modulus and Poisson's ratio, to give direct indications of the properties of the rock through which the ray paths travel. Crack density and saturation can also be calculated to determine changes in crack properties in the damaged and disturbed zones.

Appendix II provides detailed descriptions of the data acquisition and processing used during this, and past, monitoring periods. The ultrasonic array consists of twenty-four ultrasonic transducers configured as eight transmitters and sixteen receivers installed into four instrumentation boreholes using specially designed installation frames sealed within slightly expansive grout. The array is designed to provide good coverage for AE locations and provide 'skimming' ray paths so as to sample the rock immediately adjacent to the deposition hole wall. ASC's InSite Seismic Processor [*Pettitt et al.*, 2005], has been used to automatically process both the AE and ultrasonic survey data. Appendix III A and Appendix III B give the processing parameters used. Data from daily ultrasonic surveys has been automatically picked and arrivals cross-correlated to a reference survey for high-precision measurements of P- and S-wave velocity changes through the experiment. Arrivals of AEs have been manually picked and three dimensional source locations have been calculated.

2 Specific Objectives

This six-month period of ultrasonic monitoring in the Prototype Repository Experiment, has been undertaken with the following objectives;

- Produce accurate source locations for AEs so as to delineate the spatial and temporal extent of any brittle microcracking within the rock mass around the deposition hole and locate any movements on pre-existing macroscopic fractures;

- Conduct regular ultrasonic surveys to assess the effect of heating and other environmental changes on the velocity and amplitude of transmitted ultrasonic waves;

- Investigate changes in dynamic moduli and crack density to show how the properties of the rock volume around the deposition hole change through the experiment;

- Relate the AE and ultrasonic measurements to the measured *in situ* stress regime and other operating parameters such as temperature and fluid pressure;

- Outline how the results from this reporting period relate to previous monitoring periods, and into the overall experimental aims and objectives.

3   Results

3.1   Ultrasonic surveys

An indication of major environmental changes occurring in the tunnel and deposition holes can be ascertained from the temperature and pressure measurements supplied by SKB (*Goudarzi*, 2008). The temperature in the rock around the deposition hole is shown in Figure 3-1. The temperature on these instruments remains very stable over the six month monitoring period increasing by only 0.1 - 0.2 °C.

Figure 3-2a shows total pressure in the tunnel backfill above the deposition hole. A data logger problem in section 2 of the Prototype repository has meant that pressure data cannot be used between 23rd June and 11th September 2007. Boring of a new tunnel close to the Prototype tunnel is believed to have caused a loss of data (*Goudarzi*, 2008). The total pressure in the backfill over deposition hole DA3545G01 (Figure 3-2a) increases by an average of 0.35 MPa to 20th May 2007. A sudden small decrease (average of 0.15 MPa) is observed over the next two days. The pressure then rises again, reaching a peak on 2nd June 2007. A decrease occurs until 15th June 2007. Prior to the break in recording pressure, it was increasing.
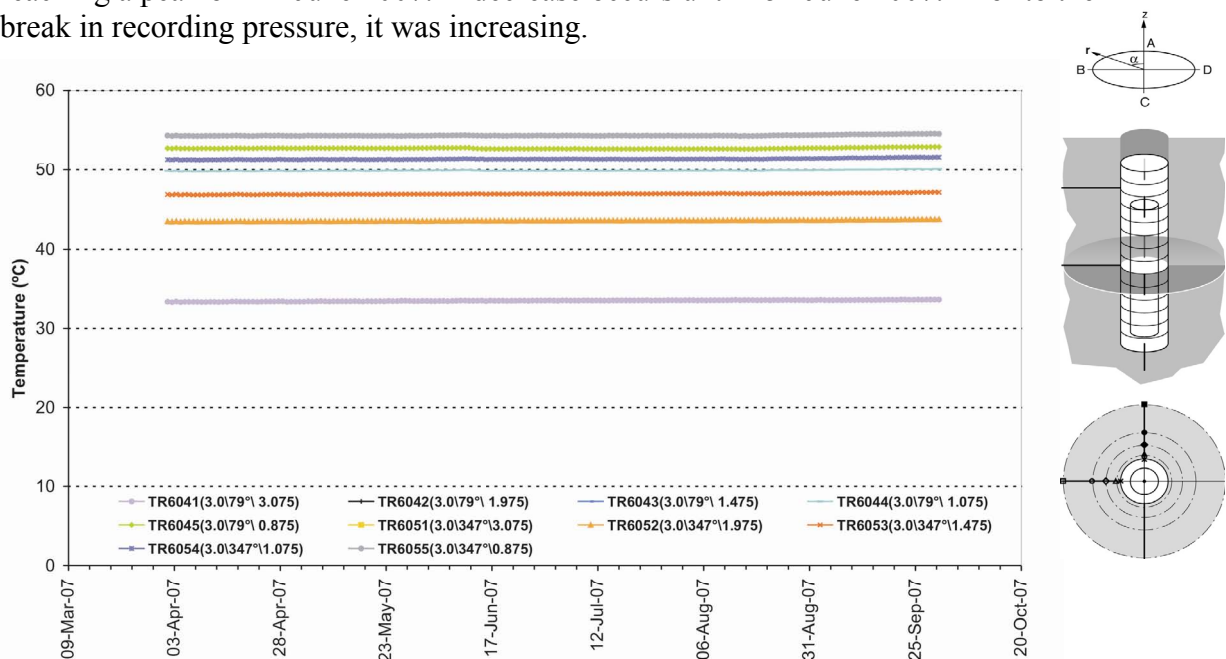
Figure 3-1: *Temperature around deposition hole DA3545G01. The sensors are positioned mid-way up the deposition hole with different depths into the rock mass (see right-hand inset) [Goudarzi, 2007].*

A constant increase in the pressure of deposition hole DA3545G01 is displayed in Figure 3-2b. Also in this case we don't have data between 1st June and 18th June 2007, followed by the recordings of 4 days and then no data for the rest of the reporting period. The only data available across the entire monitoring period are those of UB610 and show the same path of the total pressure in the tunnel backfill above the deposition hole (Figure 3-2a) followed by a decrease of pressure after 1st June 2007. Some minor variations (~0.15) occur at the end of July.

25

Velocity changes are measured between transmitter-receiver pairs on the daily ultrasonic surveys using a cross-correlation technique that allows a velocity resolution of ±2 m.s^{-1}. The reference survey for processing ultrasonic results for the previous monitoring periods, with manual P- and S-wave arrival picks, is recorded on 8th December 2004 [*Haycox et al.*, 2006a]. Processing of data recorded during this monitoring period has used the same reference survey so that results can be accurately related to previous periods. Knowing the transmitter and receiver locations, the ultrasonic velocity for each ray path was calculated with an estimated uncertainty of ±30 m.s^{-1} (±3 data points). A cross-correlation procedure was then used to automatically process subsequent surveys. This technique cross-correlates P- and S-wave arrivals from a transmitter-receiver pair with arrivals recorded on the same transmitter-receiver pair on the reference survey. This results in high-precision measurements of P- and S-wave velocity change, with estimated uncertainties of ±2 m.s^{-1} between surveys on individual ray paths. The main reason for the reduction of uncertainty when using the cross-correlation procedure is the dependency of manual picking on the user's judgement of the point of arrival. This can usually be quite indiscriminate because of random noise superimposed on the first few data points of the first break. The cross-correlation procedure then allows for a high-resolution analysis to be performed and hence small changes in velocity to be observed. This is extremely important when changes in rock properties occur over only a small section (5%) of the ray path.

Average P- and S-wave velocity change is shown in Figure 3-3a. We observed an increase in velocity between 20th and 24th April 2007. The increase in peak velocity is of a similar order for both P- and S-wave (0.5 m.s^{-1}), and can be related to the increase in pressure in the backfill over the deposition hole as display in Figure 3-3b The velocities remain more or less constant until 6th May 2007 when a sudden increase occurs over one day. P-wave peak velocity increases by 0.6 m.s^{-1} while S-wave peak velocity increases about 0.15 m.s^{-1}. After this jump the velocities increase constantly and then on 25th June 2007 we have another sudden change. Again the jump occurs over one day and affects P-waves more than S-waves: P-wave decrease of about 1.0 m.s^{-1} and S-wave decrease of 0.4 m.s^{-1}. Then velocities remain almost constant over the following three months of the monitoring period varying by only 0.2 to 0.3 m.s^{-1}. Similar changes in velocity over one day have been noted in previous monitoring periods [*Haycox et al.*, 2005b: *Haycox et al.*, 2006a,b]. The magnitude of the average changes is less than the velocity resolution of 2 m.s^{-1} estimated for ultrasonic measurements but changes on individual ray paths are significant. For example, the largest magnitude increase in velocity is observed on raypath transmitter 7 to receiver 6. P-wave velocity increases by 34.4 m.s^{-1} and S-wave velocity increases by 7.8 m.s^{-1} between 25th and 26th April 2007.

Amplitude change for this monitoring period is shown in Figure 3-3b. P- and S-wave amplitudes increase between the 20th and 26th April. The increase is high especially for P-waves which increase by 1.0 dB, while S-waves increase by 0.3 dB. As for velocity change, this can be related to the increase in pressure in the backfill over the deposition hole. Subsequently, the amplitudes exhibit a relatively constant increase. P-waves increase to a greater extent, ending the monitoring period 1.5 dB greater than at the start. S-waves increase by 0.6 dB over the six months.

The changes in amplitude and velocity between the 20th and 24th April 2007 have been further investigated by looking at the waveforms. An example of how one waveform changes is presented in Figure 3-4a. We examined ray path transmitter 7 to receiver 6, as all the ray-paths related to sensor number 6 present high variations in velocity and amplitude. As shown in Figure 3-4a, waveforms after 24th April are more energetic thus resulting in amplitude up to 3 times larger than the previous waveforms. The rapid increase of the pressure in the deposition over April 2007 (Figure 3-2a) hole results in significant changes to the character of many recorded waveforms with an increase in amplitude. With the increase in the pressure the attenuation of the ultrasonic waves is reduced meaning that they can pass more efficiently through the rock medium. The reduction in attenuation is either a result of an increase in saturation in the rock mass (fluids are pushed into microcracks and pore spaces), or a result of a reduction in crack density caused by a closing of pre-existing microcracks, or a combination of the two. Similar changes were noted also in previous reporting periods (e.g. *Haycox at al.*, 2005b).

The cross correlation, Figure 3-4b-c, shows how before the increase in amplitude, the waveforms are faster as there is a displacement to the left, both for P- and S-arrivals (Figure 3-4b and c). Such change can be interpreted as a localised change in the general rock properties rather than a systematic change in the measurement devices used in the project as different transmitter-receiver raypaths pairs are affected.
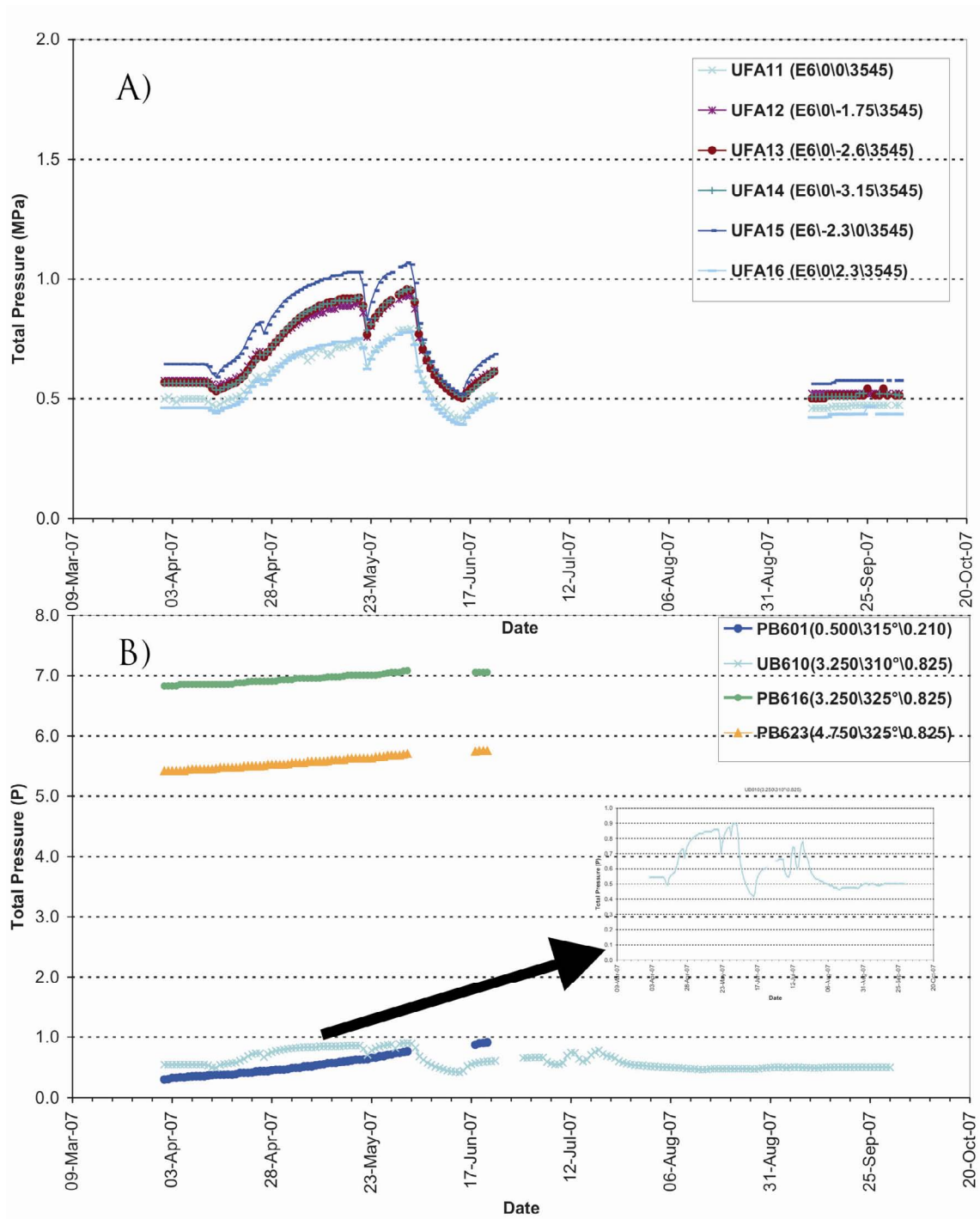
Figure 3-2: *Total pressure in (a) the backfill over deposition hole DA3545G01.*
No data are available between 24/06/2007 and 09/09/2007; (b) the rock adjacent to
deposition hole DA3545G01 [Goudarzi, 2007]. After 01/06/2007 we have data only for
UB610.
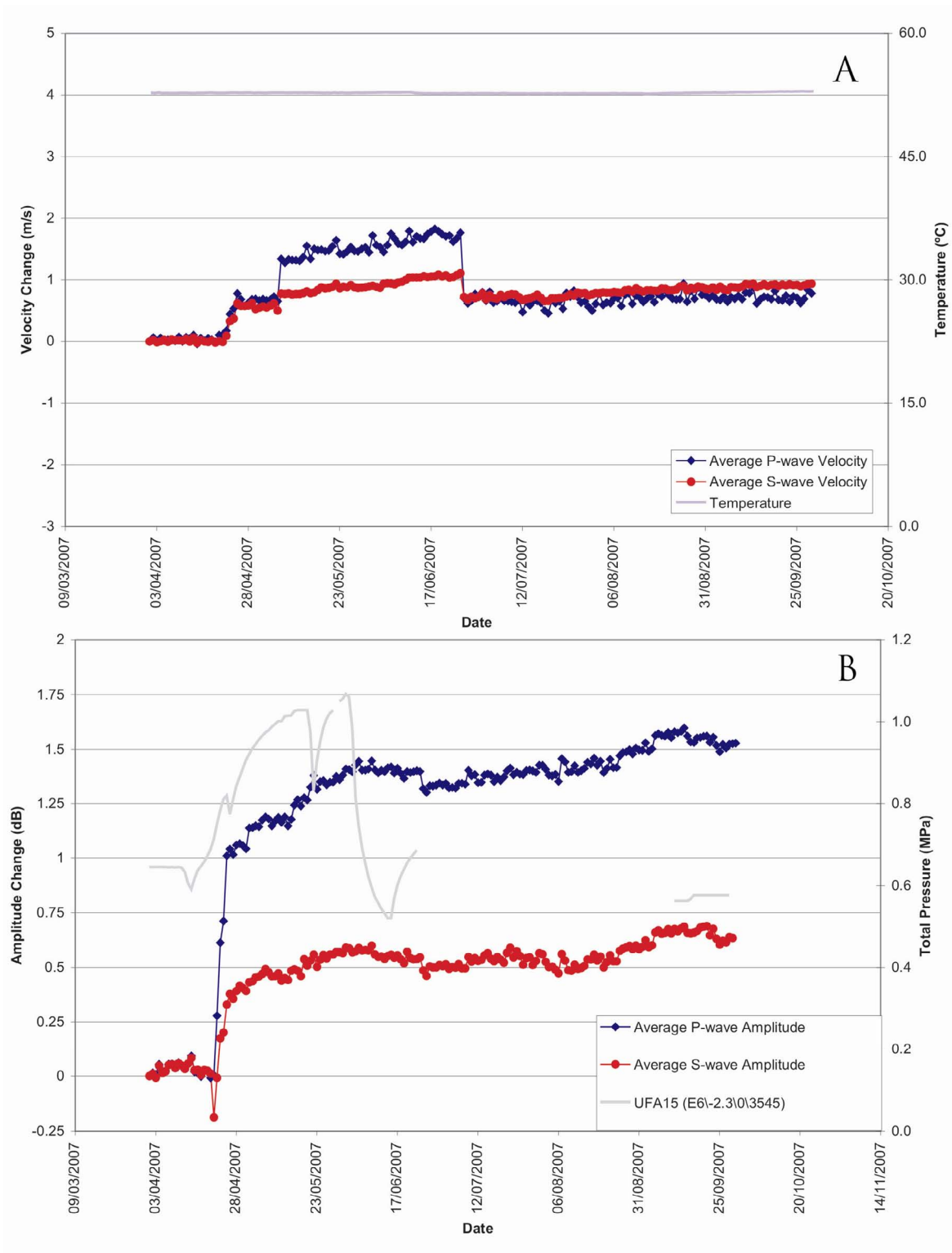
Figure 3-3: *Average P- and S-wave (A) velocity change and (B) amplitude change, for the reporting period. Temperature (TR6045) and total pressure (UFA15) are displayed on the secondary axes.*
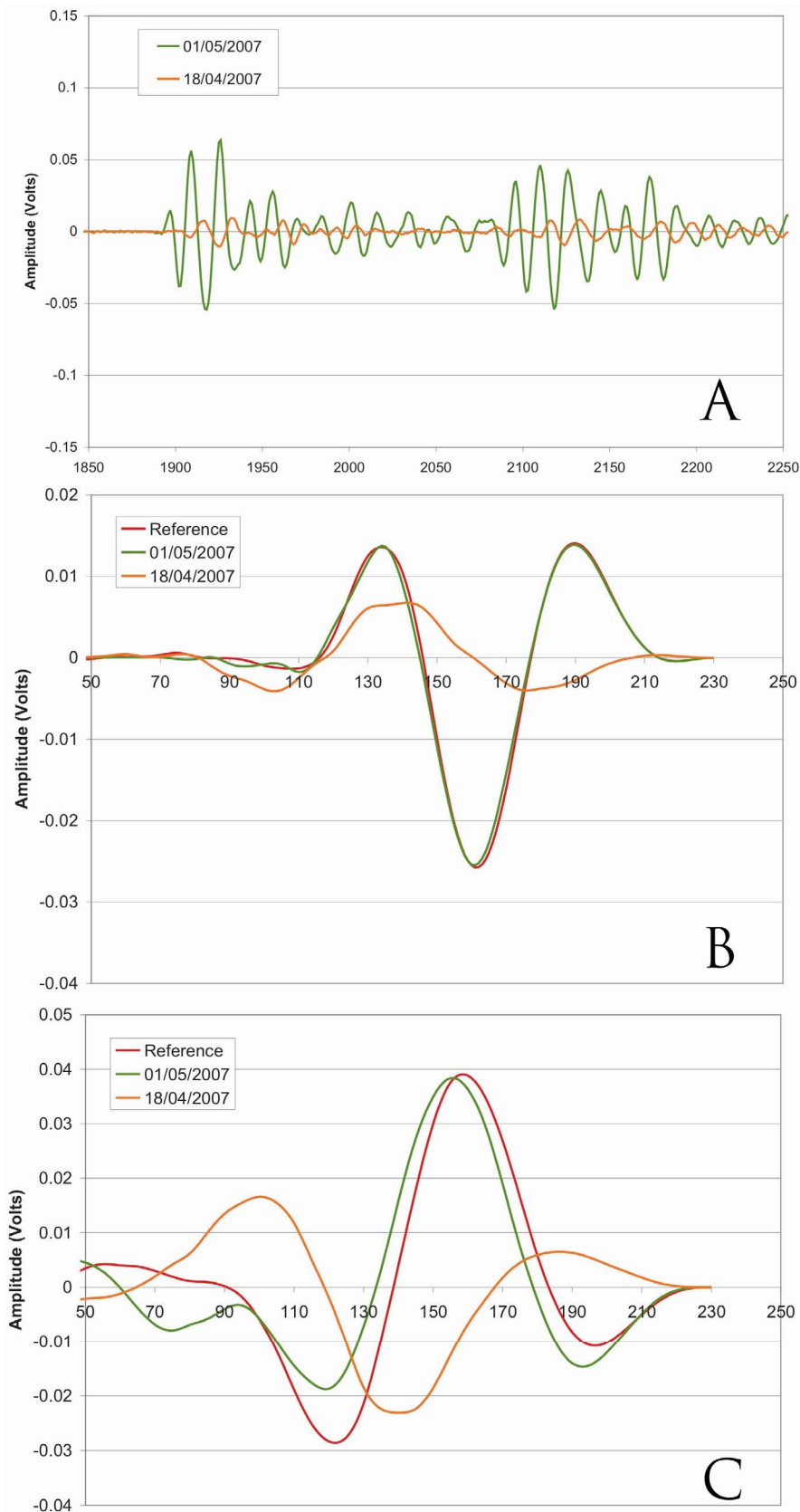
Figure 3-4: *Example plots of (a) raw waveform data points and P-waves (b) and S-waves (c) cross correlation windows for the ray path transmitter 7 to receiver 6 on 18th April and 1st June 2007. The red curve shows the reference survey from 8th December 2004.*

Pettitt et al.[1999] categorised ray paths from ultrasonic surveys into six types depending on their orientation with respect to the deposition hole and the in situ stress field (Figure 3-5). This figure shows an interpretation of the ultrasonic results in terms of disturbed and damaged regions around the void during the excavation phase of the experiment. *Pettitt et al.*[2000] undertook three-dimensional elastic stress modelling to describe these zones of stress.

Example ray paths from category 'S3' are presented in Figure 3-6. These ray paths pass within centimetres of the deposition hole through the excavation damaged zone, in a region of low compressive or tensile stress. These particular ray paths have been chosen because they provide a comparison of velocity changes down the length of the deposition hole. Each plot of velocity change is accompanied by a schematic diagram giving a perspective of the region through which the ray path passes. For all the four ray paths, very little velocity change is recorded for both P- and S-waves except for ray path 1-6. In this period we have a rapid increase of P- and S-waves over one day at the end of April 2007. In particular, P-wave velocity increases by 23 m.s^{-1} on ray-path transmitter 1 to receiver 6. Further analysis of ray paths related to this velocity increase will be presented later in this section.

Figure 3-7 shows velocity results for ray paths of category 'S1'. These ray paths pass through a region of high compressive stresses and permanent damage close to the deposition hole wall imaged by relatively high AE activity during excavation. The ray paths generally show a significant increase in velocity at the end of April 2007, for both P- and S-waves. Then velocities remain almost constant over the remaining monitoring period.

Figure 3-8 shows P-wave velocity for a selection of ray paths for which the P-waves show a velocity increase in late April 2007. The increase in velocity and amplitude at the end of April 2008 could be related to the increase in pressure as previously mentioned. This is clearly visible for most of the ray paths using both P- and S-waves. We plot the ray-paths selected for Figure 3-8 in Figure 3-9. There is no obvious relationship between the effected ray paths and zones of induced stresses from the excavation. The values of the changes are reported in Table 3-1.
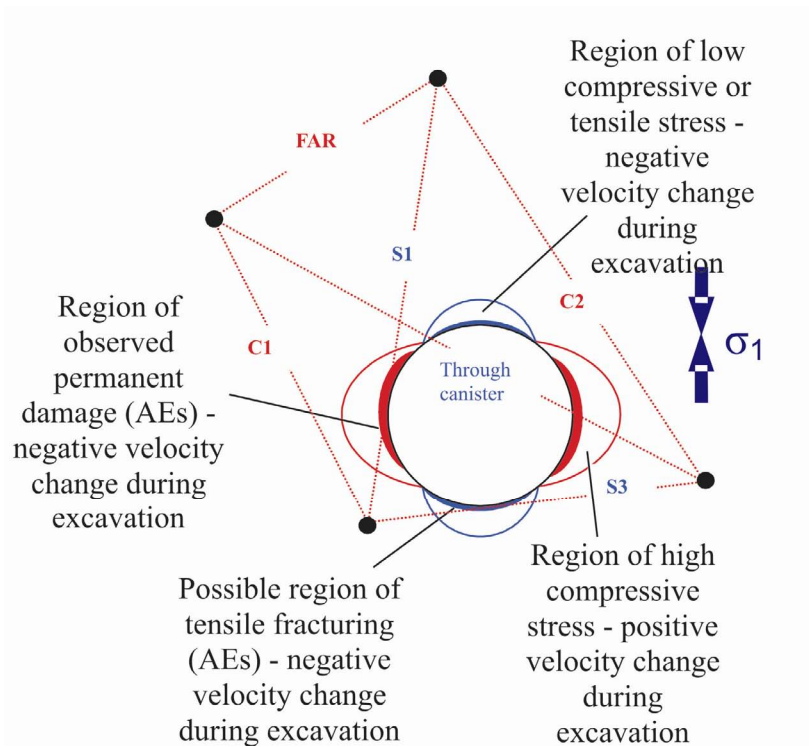
Figure 3-5: *Interpretation of the ultrasonic results during excavation in terms of disturbed and damaged regions around the deposition hole. Zones of induced stress are inferred from elastic modelling and the σ₁ orientation. After Pettitt et al.[1999].*

In order to analyse consistent and small changes in the measurements, Figure 3-10 compares the results of average velocity change across the different ray path categories described in Figure 3-5. All ray path categories show the same trend increasing at the end of April and then decreasing around the end of June 2007. Between 20th and 24th April 2007 P-waves velocity increases up to 0.3 m.s^{-1} for ray path 'S3' and up to 2.0 m.s^{-1} for ray path 'Far', the most sensitive category at this change. All the ray paths reached the maximum velocity on 25th June 2007; after which a rapid decrease up to 1.0-1.5 m.s^{-1} for all the ray paths occurs.

In Figure 3-11 we show the comparison results of average amplitude change across the different ray path categories. The trend is very similar for all the ray paths. Amplitudes also show a jump at the end of April 2007. P- and S-wave amplitudes constantly increase, after this time the decrease that influences the velocity values at the end of June is not displayed in amplitudes. For P-waves the maximum increase is observed for ray path belonging to category 'C1' (1.1 dB) and the smallest increase for category 'S3' (0.2 dB). For S-waves the minimum increase is again observed for ray path belong to category 'S3' (0.2 dB) while the maximum increase is related to ray path 'C2' (0.6 dB).

Figure 3-12 shows changes in Young's Modulus, Poisson's Ratio, Crack Density and Saturation Parameters calculated from the average measured velocities for the ray path categories. 'Crack Density' and 'Saturation' of the rock mass are determined using the method of *Zimmerman and King*[1985], as described in Appendix II.

Young's Modulus and Saturation increase at the end of April and then decrease at the end of June 2007 showing the same trend as P- and S-wave velocities. Poisson's ratio shows less variation in its values. Crack density shows the opposite behaviour displaying a decrease on the end of April, followed by an increase on the end of June 2007. All the ray paths follow the same trend but the category that shows highest variation is 'Far'. These changes can be related with the rapid changes in pressure in the backfill over deposition hole DA3545G01 as shown in Figure 3-2a. While no rapid changes in temperature are recorded.

During this six month period, the velocity and amplitude results have shown an increase over few days at the end of April 2007 followed by a sudden decrease over one day at the end of June 2007. These variation are particular relevant for ray paths using receiver 6 and belonging to category 'Far'. P-waves are more sensitive to changes. From the average plots shown in Figure 3-3 the maximum variation is about 0.6 m.s^{-1} for P-wave velocity and 1.0 dB for P-waves amplitude. Similar changes were noticed during previous reporting periods (i.e. *Haycox and Pettitt*, 2005).
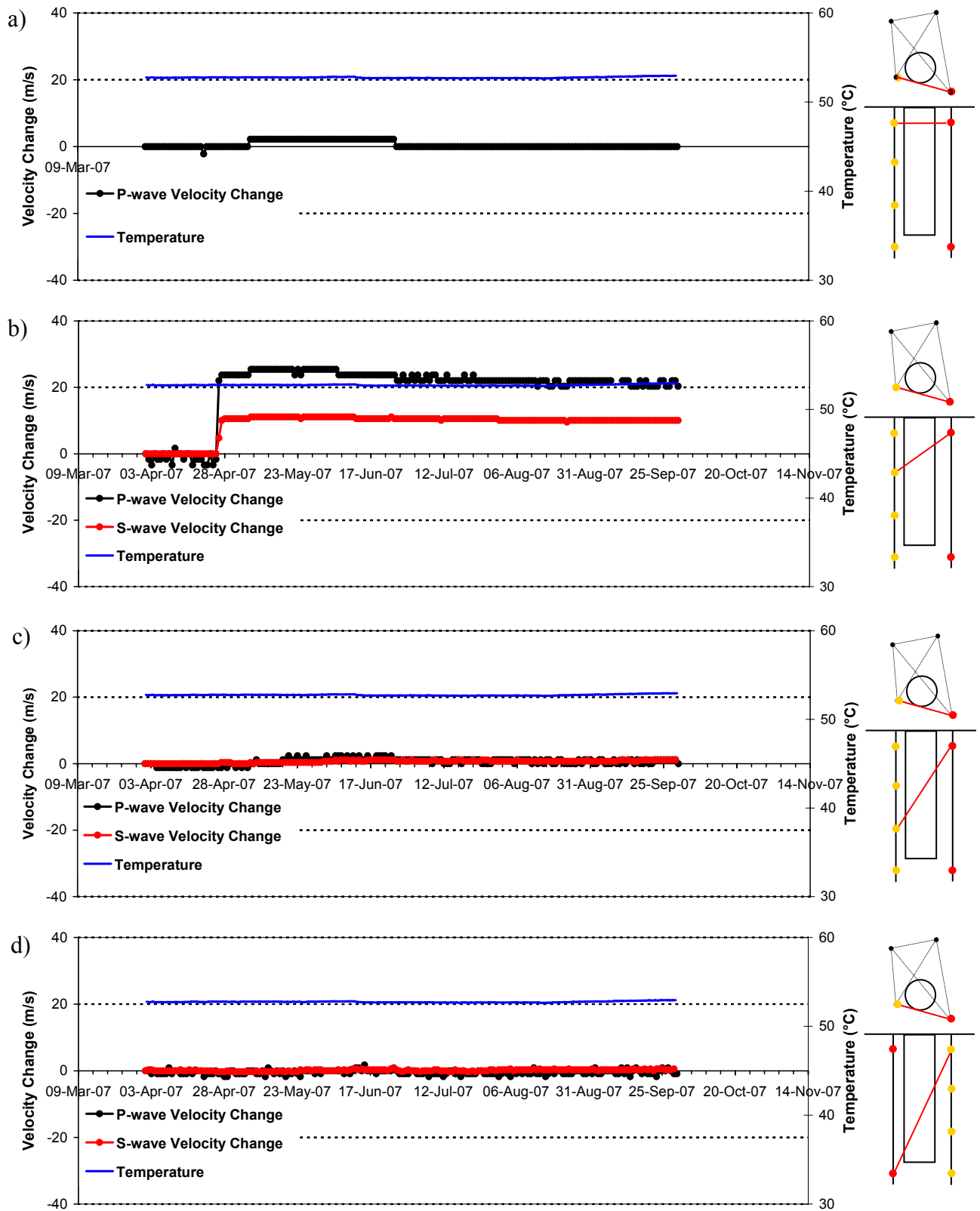
Figure 3-6: *Velocity changes measured on ray path category 'S3' (Figure 3-5) for deposition hole DA3545G01. Ray paths shown are from a top transmitter to receivers with increasing depth: a) transmitter, $t_n=1$, receiver, $r_n=5$; b) $t_n=1$, $r_n=6$; c) $t_n=1$, $r_n=7$; d) $t_n=4$, $r_n=1$. Schematic diagrams in the right margin indicate the relative positions of transmitter (red) and receiver (gold). Temperature (TR6045) is displayed on the secondary axes.*
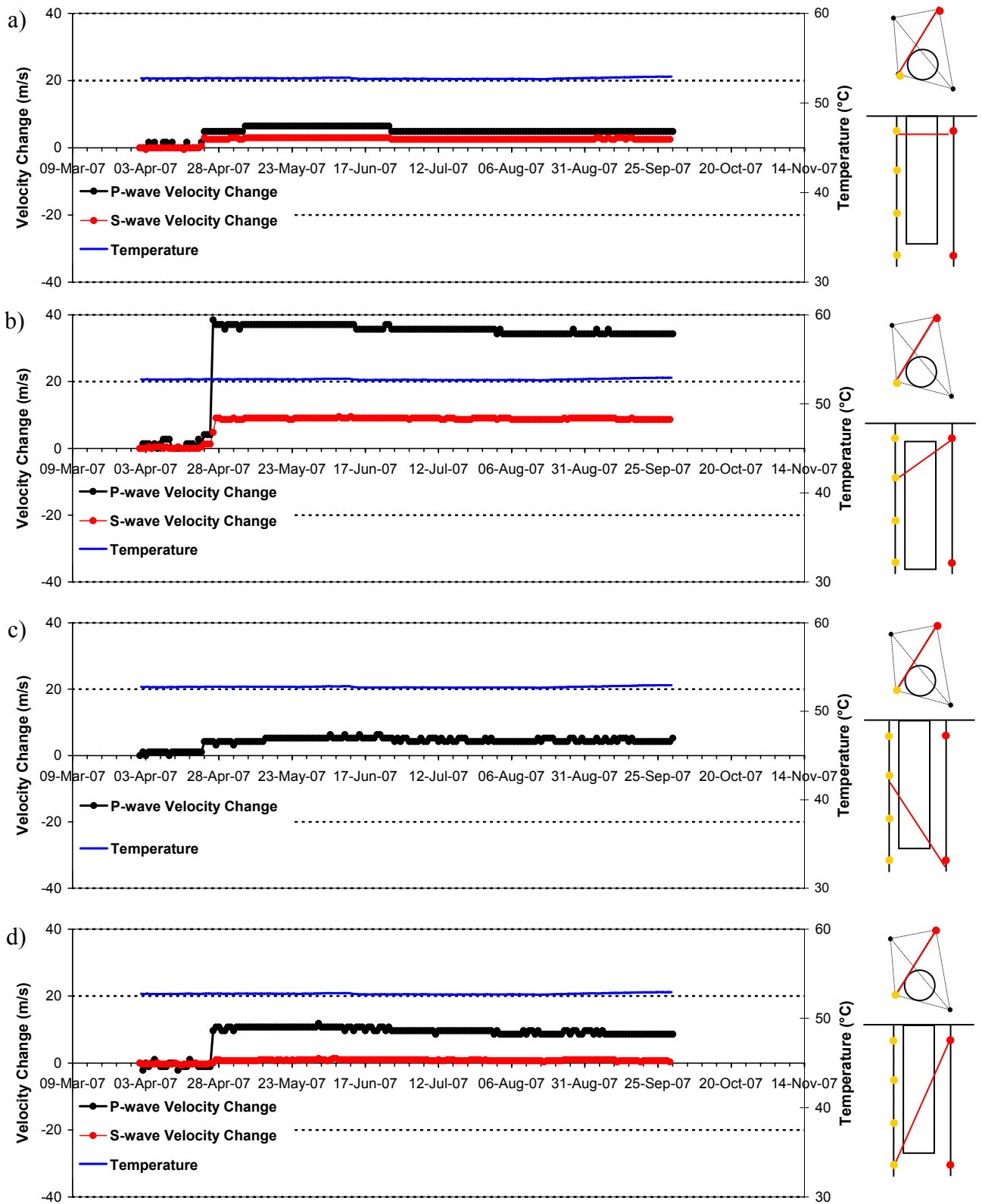
Figure 3-7: *Velocity changes measured on ray path category 'S1' (Figure 3-5) for deposition hole DA3545G01. Ray paths shown are from a top transmitter to receivers with increasing depth: a) transmitter, $t_n=7$, receiver, $r_n=5$; b) $t_n=7$, $r_n=6$; c) $t_n=7$, $r_n=7$; d) $t_n=7$, $r_n=8$. Schematic diagrams in the right margin indicate the relative positions of transmitter (red) and receiver (gold). Temperature (TR6045) is displayed on the secondary axes.*
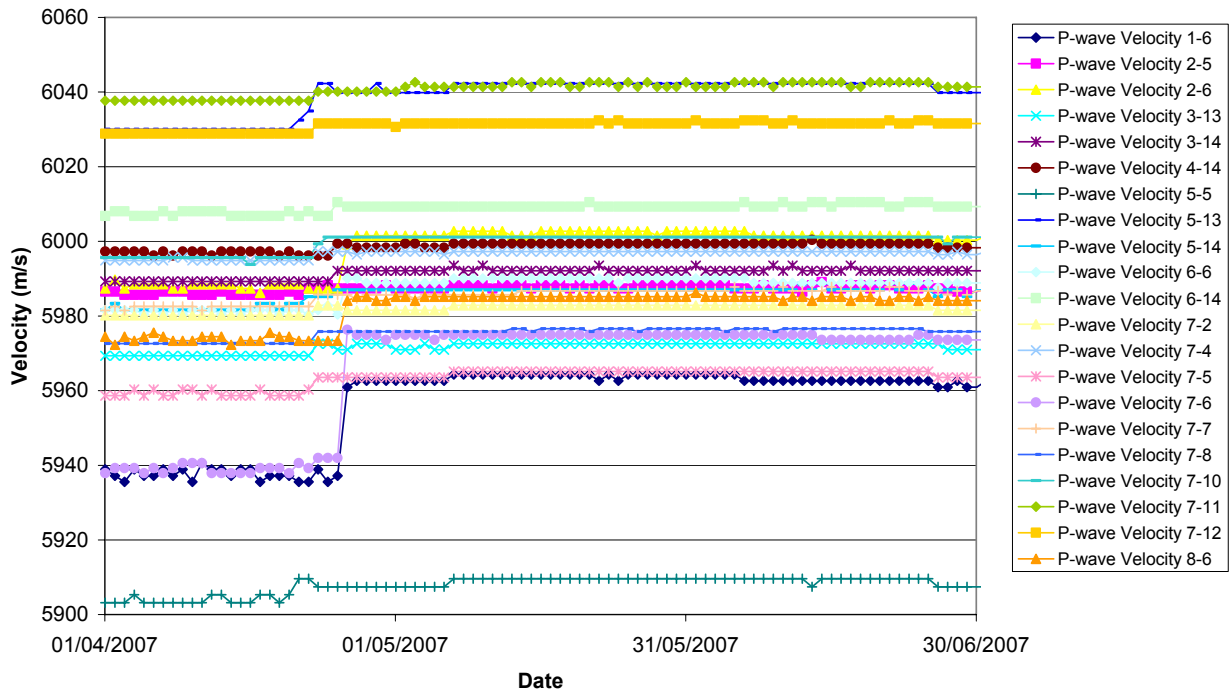
Figure 3-8: *A selection of P-wave velocity for ray paths which experience an increase in velocity at the end of April 2007. The magnitude of increase varies between the ray paths up to 35 m.s^{-1}.*
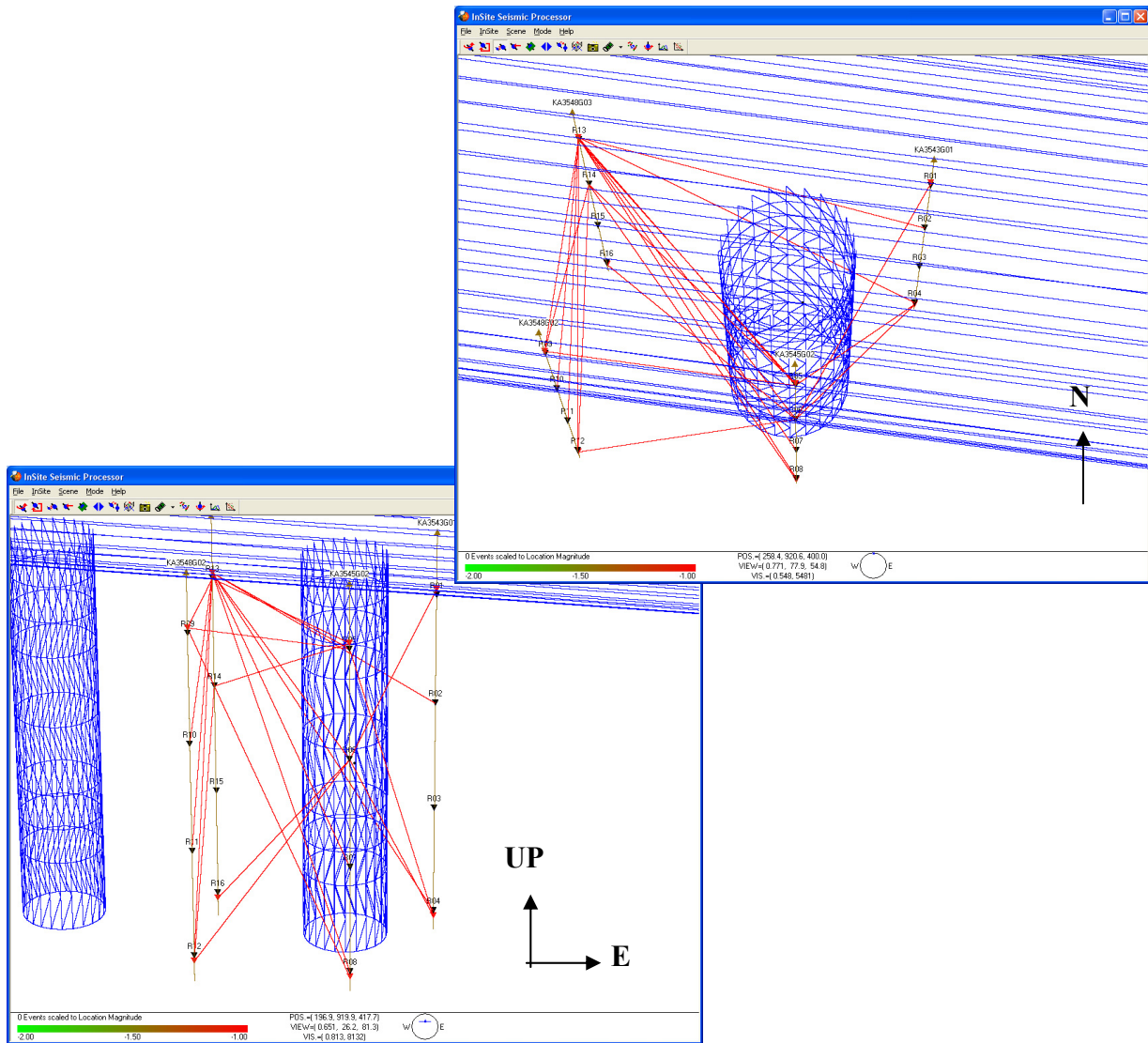
Figure 3-9: *View of a selection of ray paths used in the P-wave velocity plot shown in Figure 3-8 which experience an increase in velocity at the end of April 2007.*

Table 3-1: Difference in velocity and amplitude for P-waves for a selection of ray paths used in the P-wave velocity plot shown in Figure 3-8 which experience an increase in velocity at the end of April 2007 (changes calculated between 1st and 30th April 2007).

Raypath	Velocity change (m.s^{-1})	Amplitude change (dB)
1-6	23.7	12.7
2-5	1.7	0.2
2-6	14.2	9.1
3-13	3.3	2.1
3-14	2.8	4.8
4-14	1.1	4.8
5-5	4.3	2.9
5-13	9.8	3.9
5-14	5.4	4.5
6-6	7.2	9.5
6-14	2.5	4.6
7-2	1.3	3.3
7-4	2.4	3.8
7-5	4.9	3.9
7-6	35.7	14.7
7-7	4.2	1.9
7-8	3.2	1.9
7-10	5.5	2.1
7-11	2.5	1.5
7-12	2.7	0.8
8-6	9.7	11.9
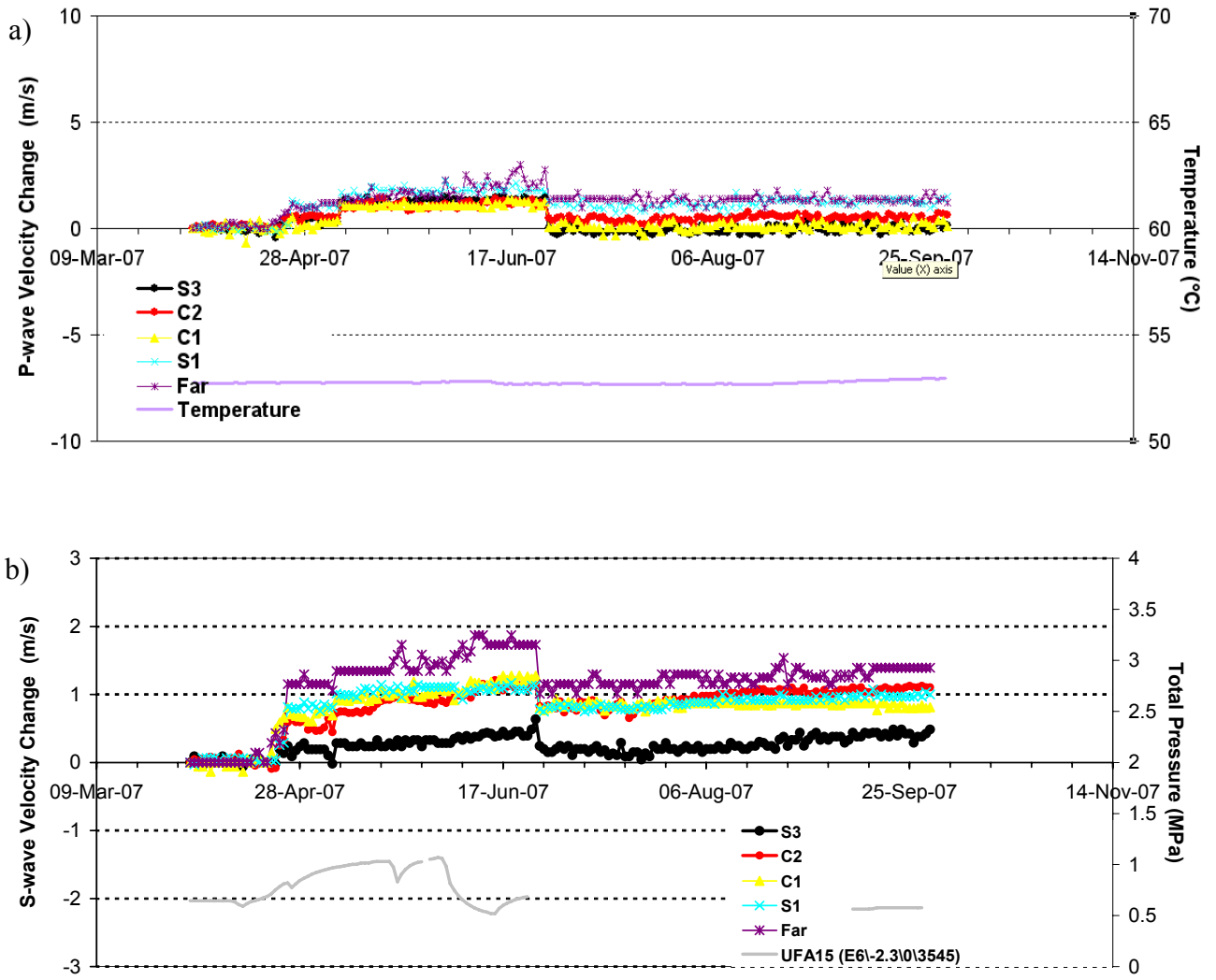
Figure 3-10: *Velocity change plots of 5 ray path categories around deposition hole DA3545G01 for (a) P-waves and (b) S-waves. Temperature (TR6045) and pressure (UFA15) are displayed on the secondary axes.*
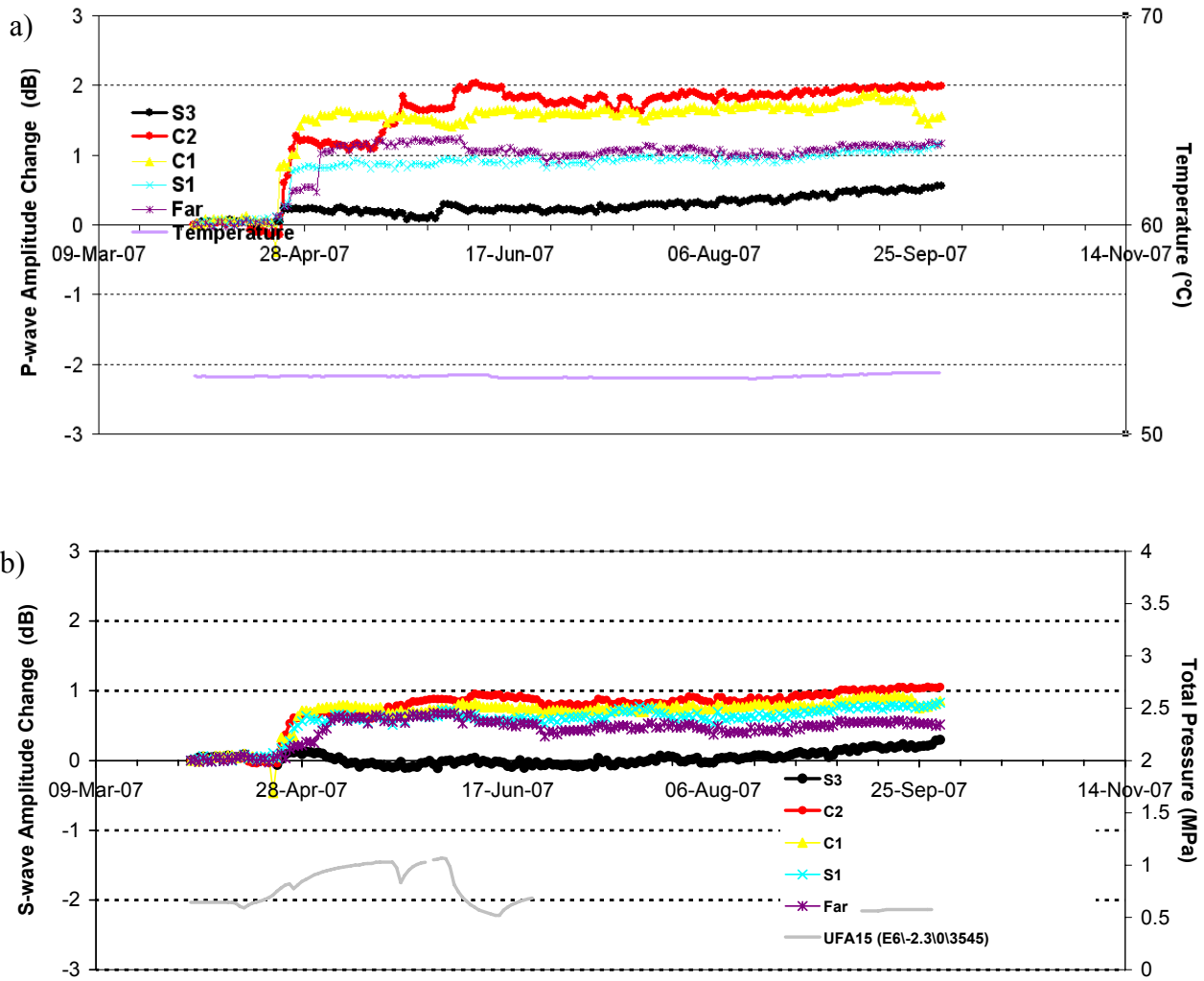
Figure 3-11: *Amplitude change plots of 5 ray path categories around deposition hole DA3545G01 for (a) P-waves and (b) S-waves. Temperature (TR6045) and pressure (UFA15) are displayed on the secondary axes.*
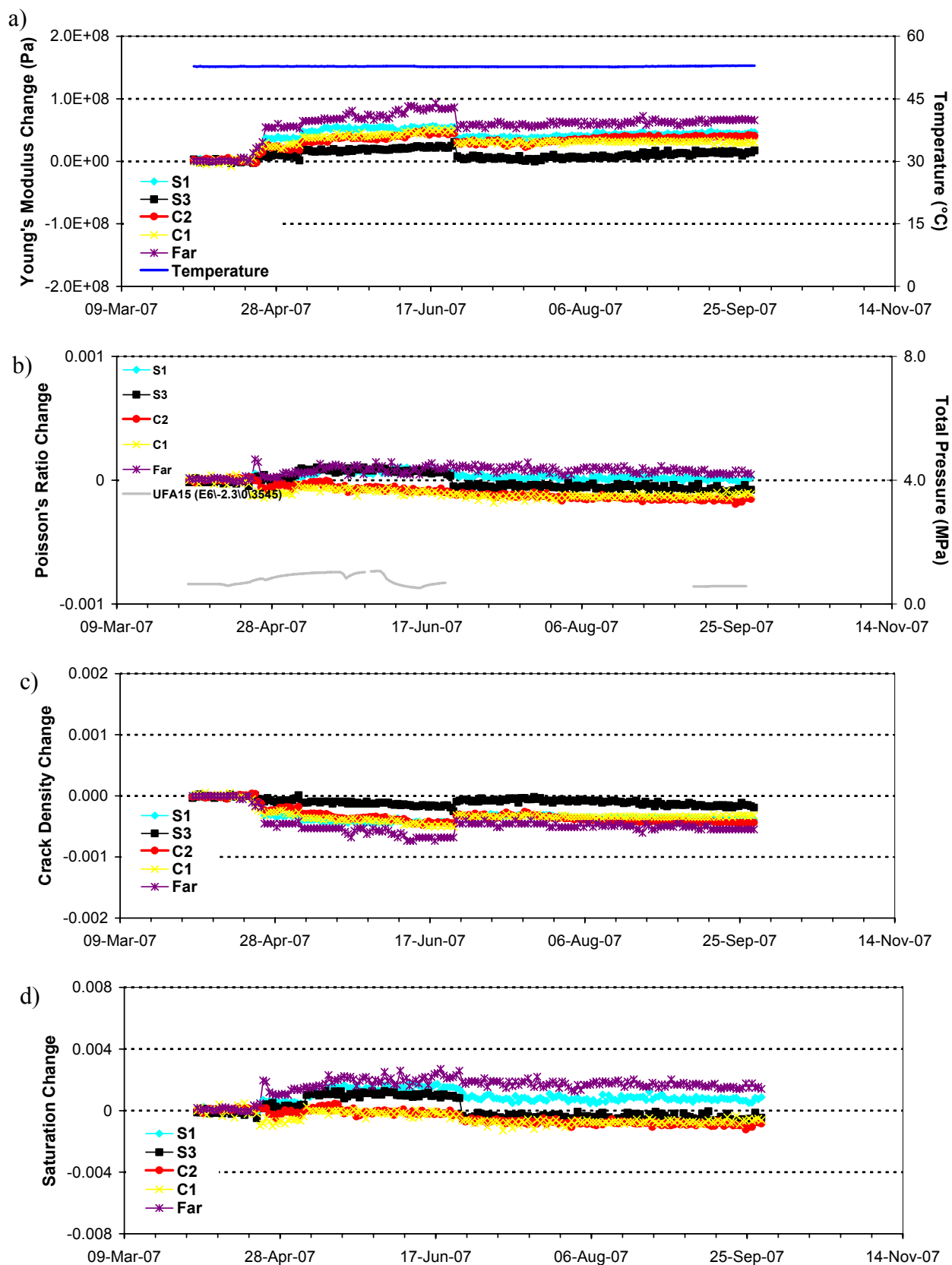
Figure 3-12: *Changes in rock parameters during this reporting period for average P- and S-wave velocity values on different ray path orientations. (a) Young's Modulus, (b) Poisson's Ratio, (c) Crack Density and (d) Saturation. Ray path orientations are described in Figure 3-5. Temperature (TR6045) and pressure (UFA15) are displayed on the secondary axes.*

3.2   Acoustic Emissions

The parameters used to process AEs are displayed in Appendix III. 115 events have been located with high confidence from 221 triggered events during this reporting period. The estimated uncertainty for these events is less than 5cm, determined using calibration 'hits' performed within the deposition holes after excavation (see Appendix II for further details).

The temporal response of triggers and located events recorded during this monitoring period is shown in Figure 3-13. A trigger is described as an event that has been acquired by the system, but may not be of sufficient energy or quality to be located during the processing procedure. 'Noise' events, produced from electrical or man-made sources, have been removed from this count to allow a more accurate representation of fracturing in the rock. The 221 temporal distributions of AE triggers is shown in Figure 3-13b while the temporal response of the 115 located AE events is displayed in Figure 3-13a. A maximum of 6 triggers are recorded on one day, on 25th April 2007. The maximum number of located events (4 events) is on 30th September 2007, while the average number is 0.63 located AE per day during this monitoring period, so we have a minor increase with respect to the previous six months (Table 3-2). There are also marginal increase in event rates during the high pressure changes in April and June.

Table 3-2: Average number of located AEs per day for six monthly periods between 1st October 2004 and 30th September 2007.

Time Period	Average Number of Events per Day
1st October 2004 to 31st March 2005	0.32
1st April 2005 to 30th September 2005	0.21
1st October 2005 to 31st March 2006	0.27
1st April 2006 to 30th September 2006	0.80
1st October 2006 to 31st March 2007	0.40
1st April 2007 to 30th September 2007	0.63

In Figure 3-14 we show the locations in relation to physical features of the Prototype Repository. Instrumentation boreholes are represented by brown vertical lines and the tunnel and deposition hole outlines are represented by blue wireframes. All the events are located in three tight clusters at a depth of approximately 455 m. Figure 3-15 shows waveform examples for each cluster. As displayed in the figure the waveforms recorded on different channels demonstrate the high quality data that is recorded using the array.

Most events (54 AEs) locate in Cluster A on the SE side of deposition hole DA3545G01. This cluster was observed in previous monitoring periods (*Haycox et al.*, 2006a,b; *Zolezzi et al.*, 2007). The centre of the events in Cluster A is N,E,D = (268.75, 921.07, 455.1) (Table 3-3). The range of values measured generally supports the accuracy of location measured by calibration hits (see Appendix II). The events are close enough together to be considered occurring on the same feature, as demonstrated by Figure 3-16a which shows a close up plan view of the events. The temporal response of these events is presented in Figure 3-17a. This shows that events in this cluster occur throughout the monitoring period. These AEs occur along the S3 ray path category that passes through a region of low-compressive or tensile stresses.

We define cluster B as the 47 events located on the SW of the DA3545G02 deposition hole (Figure 3-16b). The same cluster was revealed in the previous report *(Zolezzi et al.,* 2007). AEs are very tight and the average location is N,E,D=(269.07, 919.7, 455.97) (Table 3-4). Also this cluster occurs throughout the monitoring period (Figure 3-17b).

No evidence of cluster C (Figure 3-16c) was present in the previous six months, but some activity was recorded around this area during the excavation period of the tunnel (*Pettitt et al.*, 2000). The average location of Cluster C (14 events) is N,E,D=(269.48, 919.54, 455.046) (see Table 3-5). Figure 3-17c shows that activity in this cluster starts in June 2007.

Both cluster B and C occurs along the S1 ray path that passes through a region characterized by high compressive stresses (Figure 3-5).

Table 3-3: Values for the 54 events located in Cluster A.

	Northing (m)	Easting (m)	Depth (m)
Minimum	268.7	921.01	455.05
Maximum	268.81	921.13	455.15
Mean	268.75	921.07	455.1
Standard Deviation	0.018	0.016	0.018

Table 3-4: Values for the 47 events located in Cluster B.

	Northing (m)	Easting (m)	Depth (m)
Minimum	268.47	917.34	450.12
Maximum	269.14	919.80	455.12
Mean	269.07	919.7	454.97
Standard Deviation	0.020	0.02	0.02

Table 3-5: Values for the 14 events located in Cluster C.

	Northing (m)	Easting (m)	Depth (m)
Minimum	269.48	919.54	450.03
Maximum	269.43	919.56	455.07
Mean	269.48	919.54	455.046
Standard Deviation	0.024	0.024	0.024

Figure 3-18 shows plan views of events recorded during excavation, the initial phase of heating, the previous monitoring period and this reporting period. The majority of the events are located in the NE and SW quadrants during excavation and initial heating [*Pettit et al*., 2000; *Pettit et al*., 2002, *Haycox et al.*, 2005a]. These regions are subject to increased compressive stresses, as identified from the insitu stress field by *Pettit et al*.[1999]. Smaller clusters were observed in the orthogonal regions of low-compressive or tensile stress. It is important to note that events located during this reporting period are consistent with previous results, i.e. no events are positioned in regions where activity has not been observed in the past. In particular clusters A and B are located in the same areas of the clusters identified in the previous report, and thus they belong to the same structures. The events could be a continuation of activity in the damage zone, created either by movement on pre-existing microcracks, or as a result of extension or formation of new microcracks in the existing damaged region (see Figure 3-18). In the previous six-month report (*Zolezzi et al*., 2007) we investigated if these clusters may be related to movement of a geomechanical instrument, but no evidences of this was found. Low magnitudes characterize the entire acoustic emission data set, therefore we can assume that the rock mass around the deposition holes has remained stable during this six-month period (Figure 3-19).
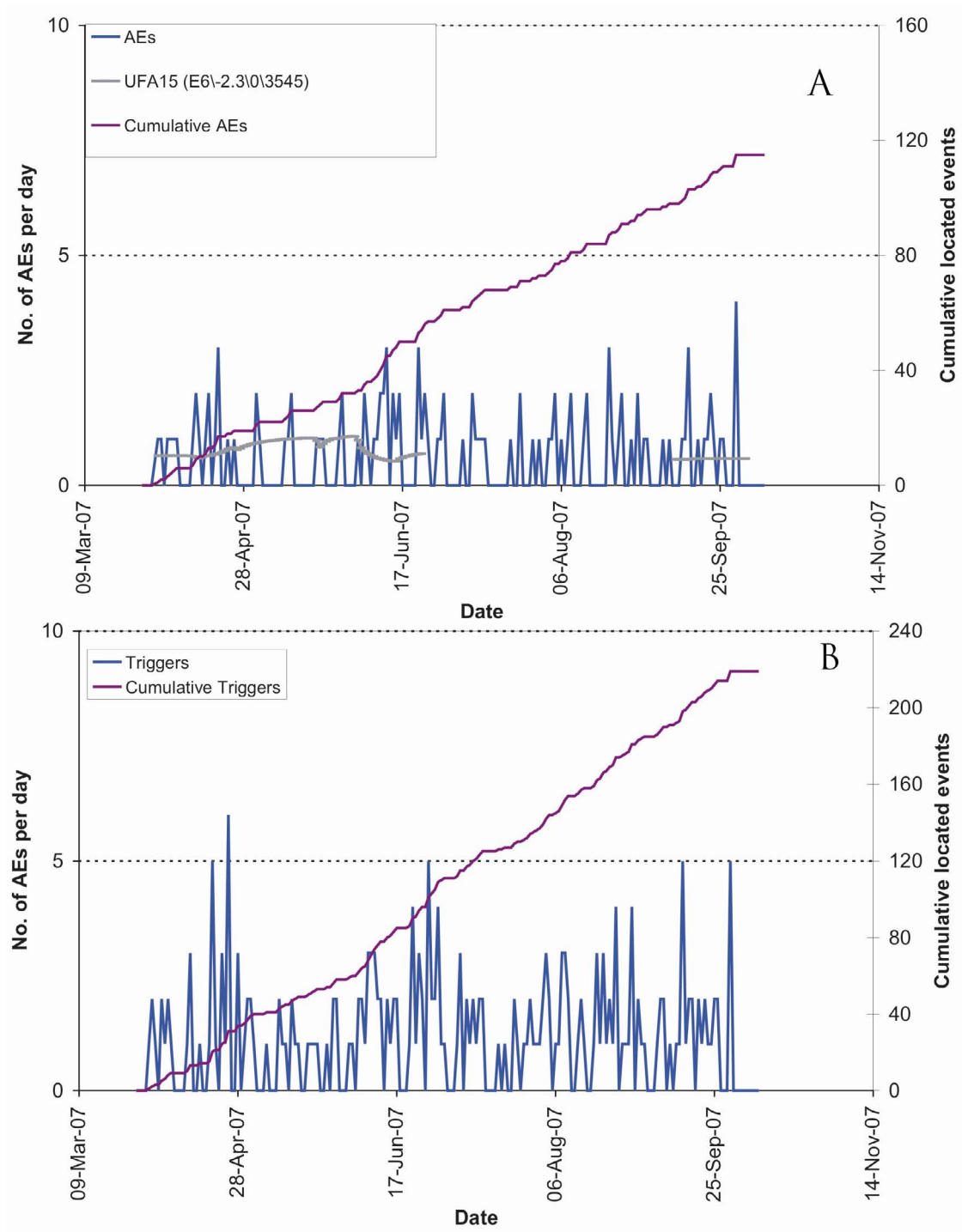
Figure 3-13: *Temporal response plot of located AE (a) and AE triggers (b); number per day on left axes and cumulative number right hand axes. In figure (a) we plot also the pressure (UFA15) to show how the first increase in AE events and triggers can be related to pressure increase.*
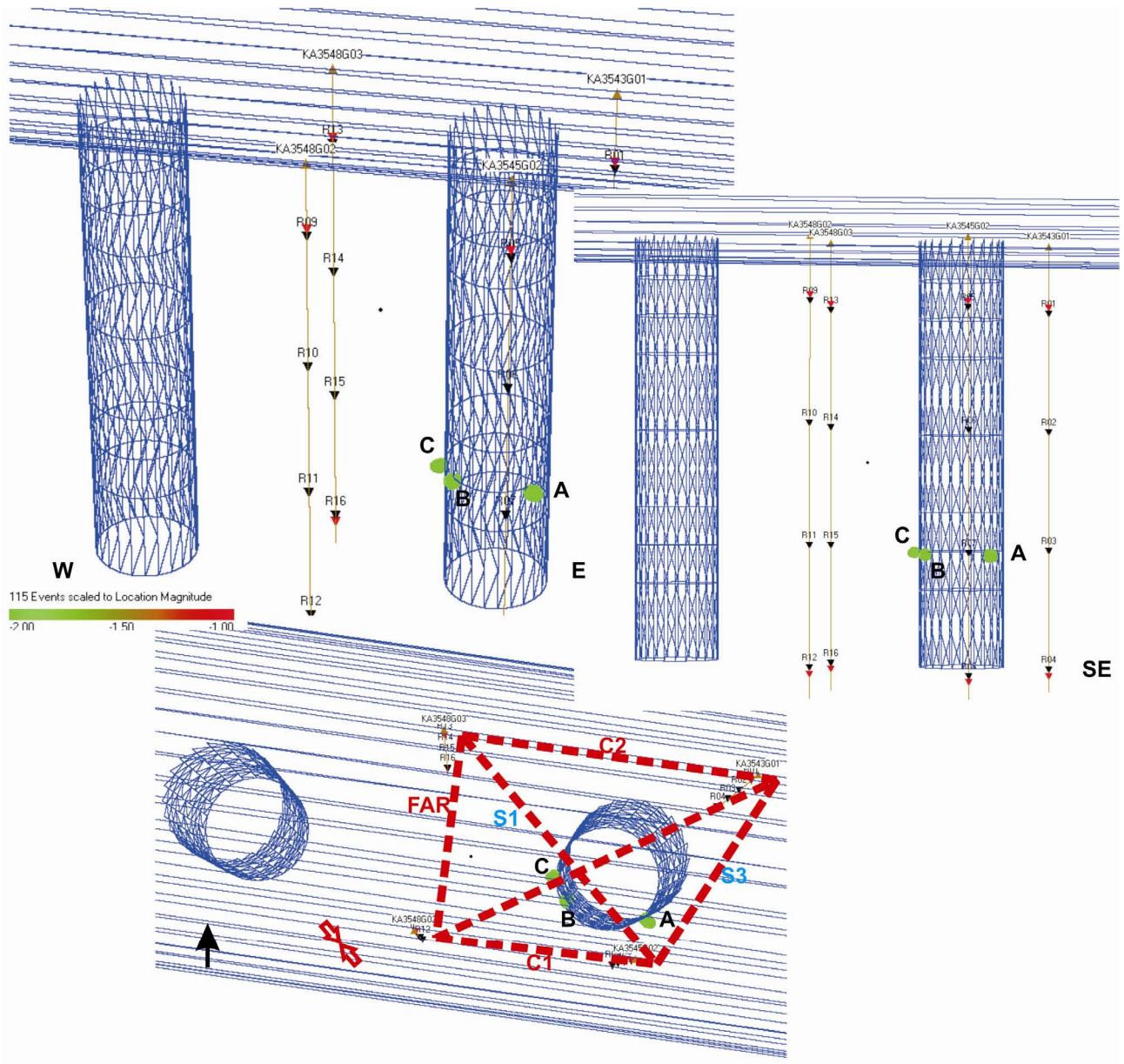
Figure 3-14: *Three views of AE activity located around deposition hole DA3545G01. (Top: Oblique view looking North; Middle: Transverse view looking north; Bottom: Plan view). The different ray paths used in the ultrasonic survey are also shown.*
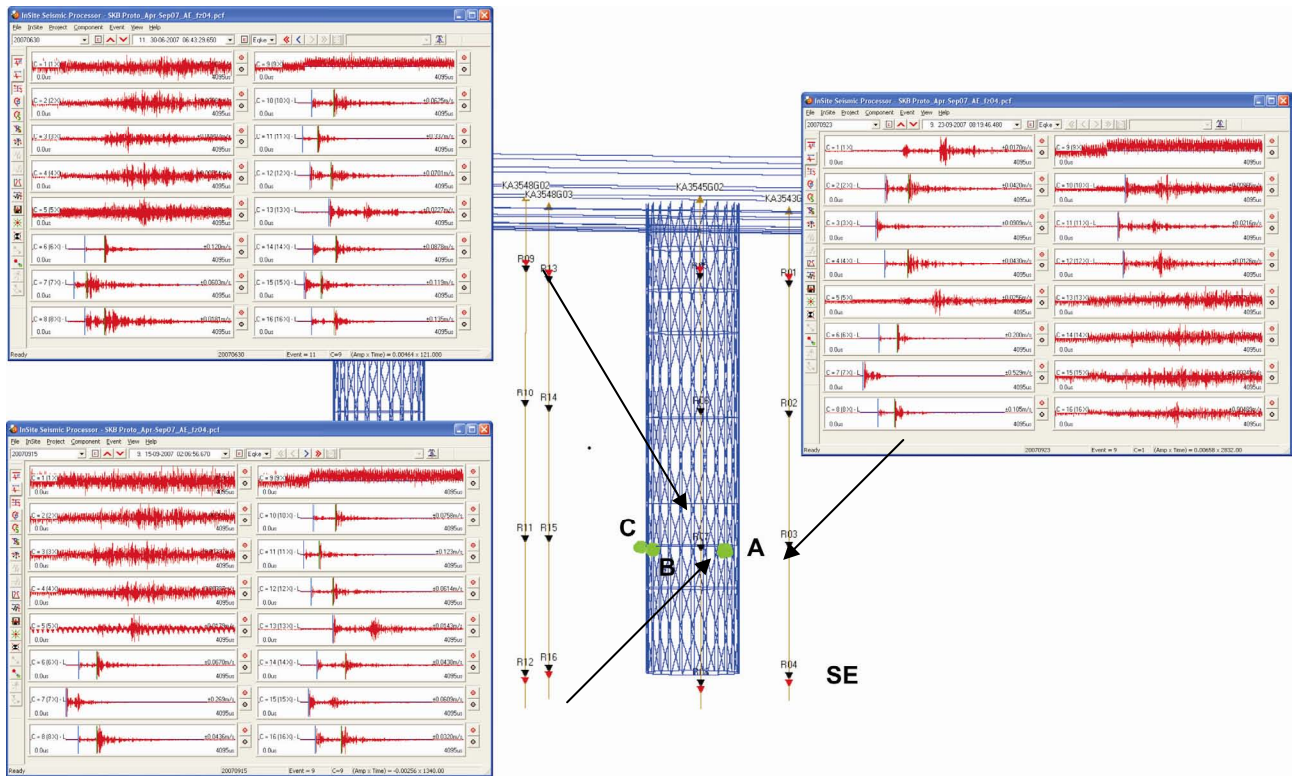
Figure 3-15: *Waveforms from selected events shown in relation to a transverse view of AE activity.*
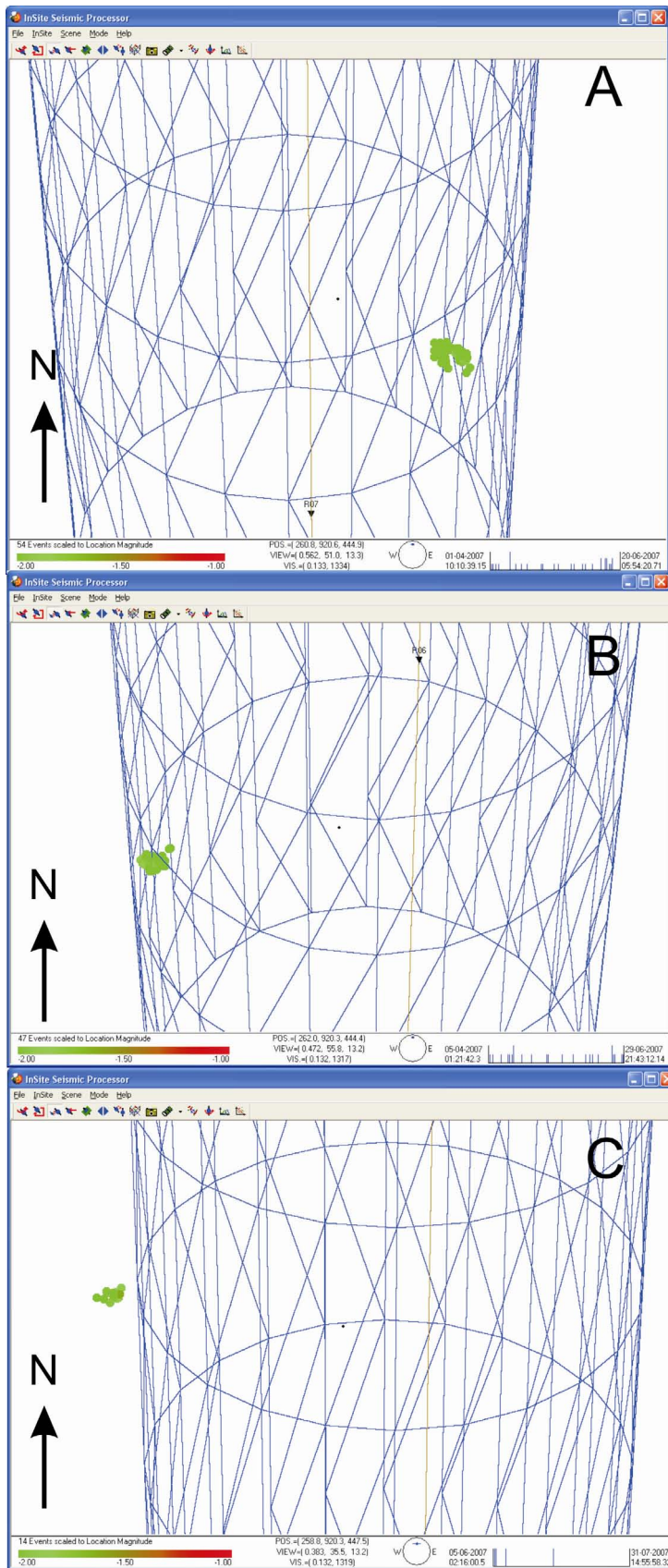
Figure 3-16: *Close up view of A) Cluster A containing 54 events; B) Cluster B containing 47 events; C) Cluster C containing 14 events.*
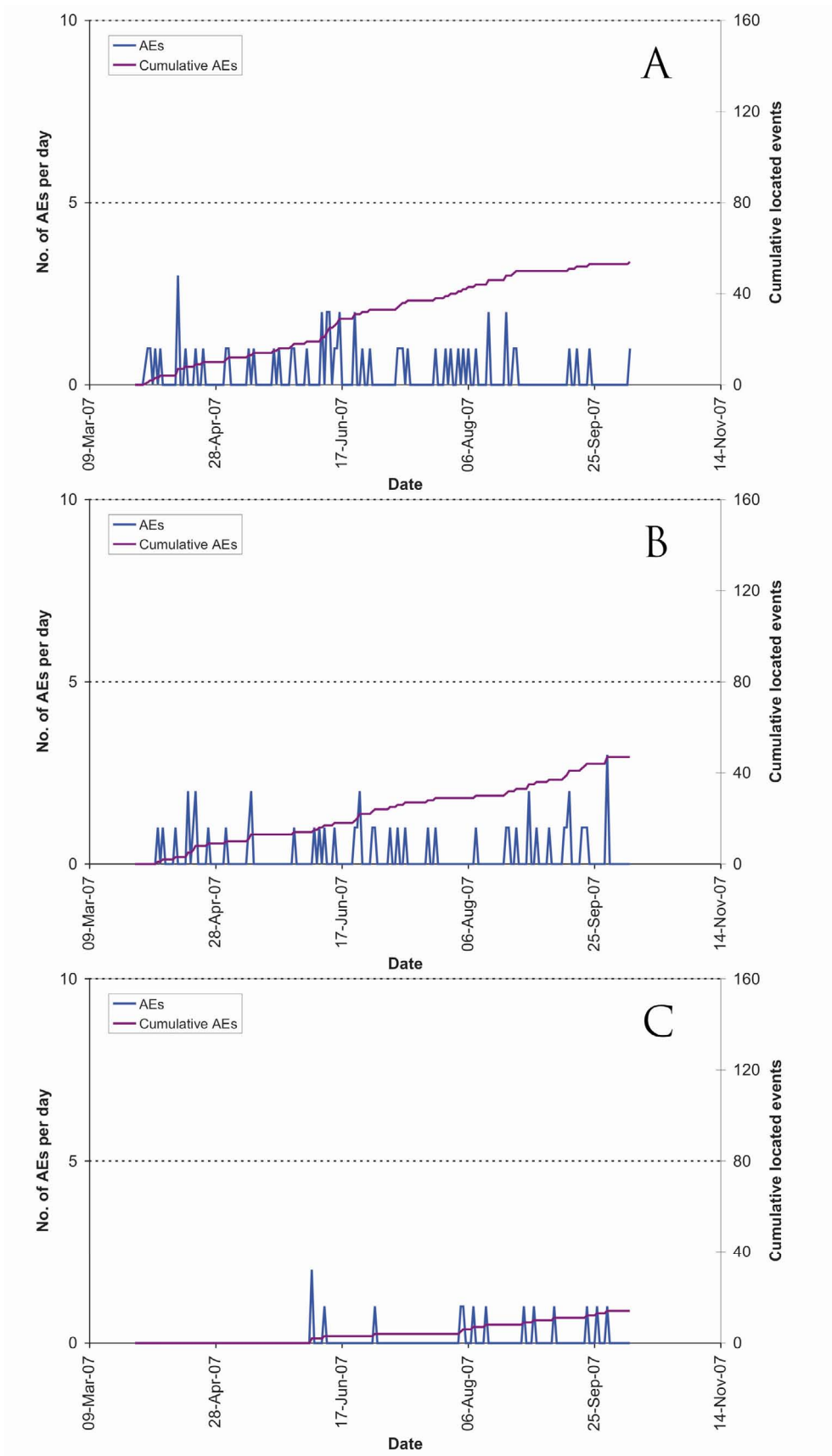
Figure 3-17: *Temporal response plot of located AEs in the identified clusters for a) Cluster A; b) Cluster B: and c) Cluster C. The plots show number per day on left axes and cumulative number right hand axes.*
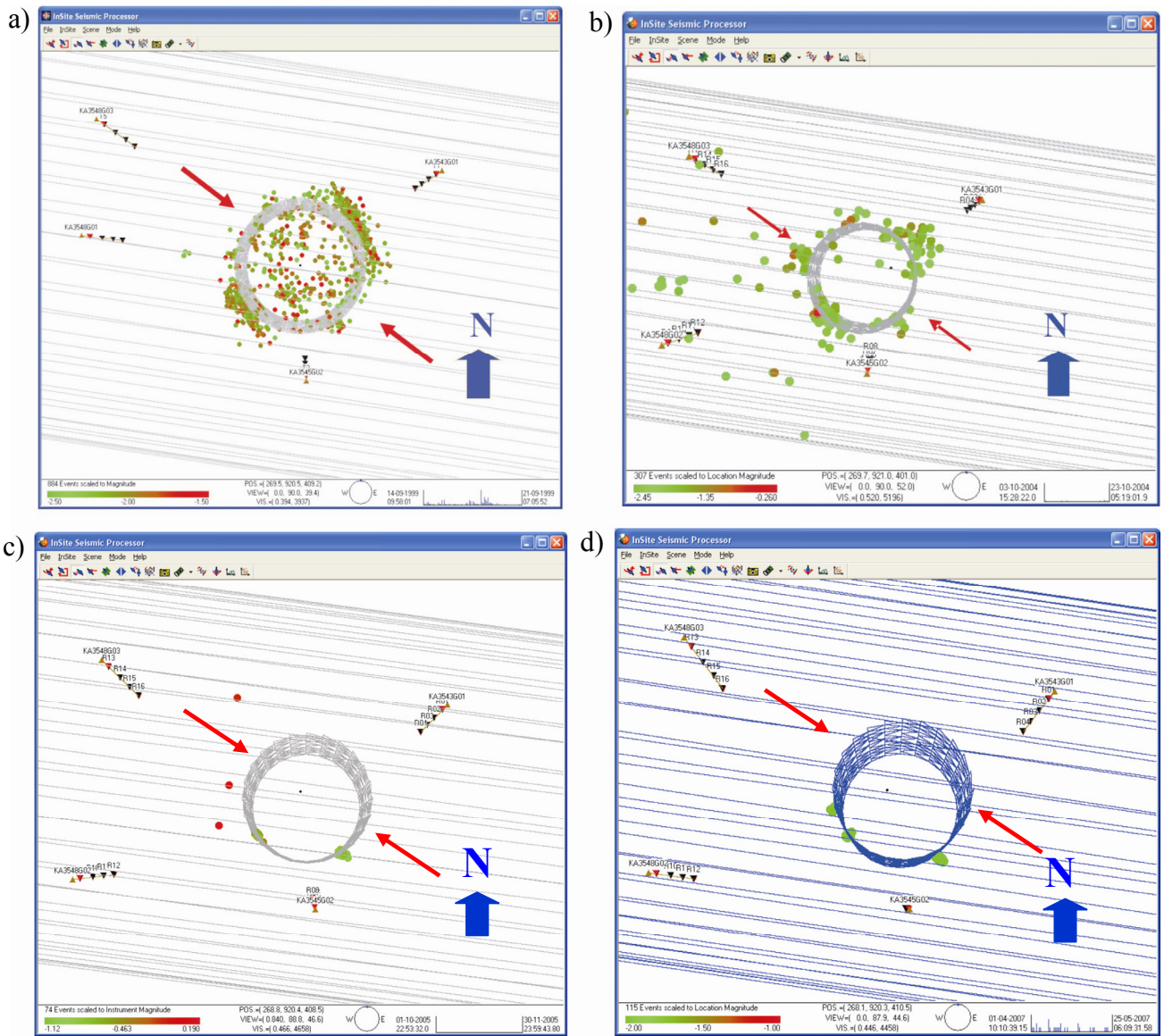
Figure 3-18: *Plan view of AEs located around deposition hole DA3545G01 during (a) the excavation phase, (b) monitoring during heating to 31/03/2006, (c) monitoring phase during heating, from 01/10/2006- 31/03/2007 (d) this reporting period (01/04/2007- 31/09/2007). The red arrows mark the orientation of the principle stress.*
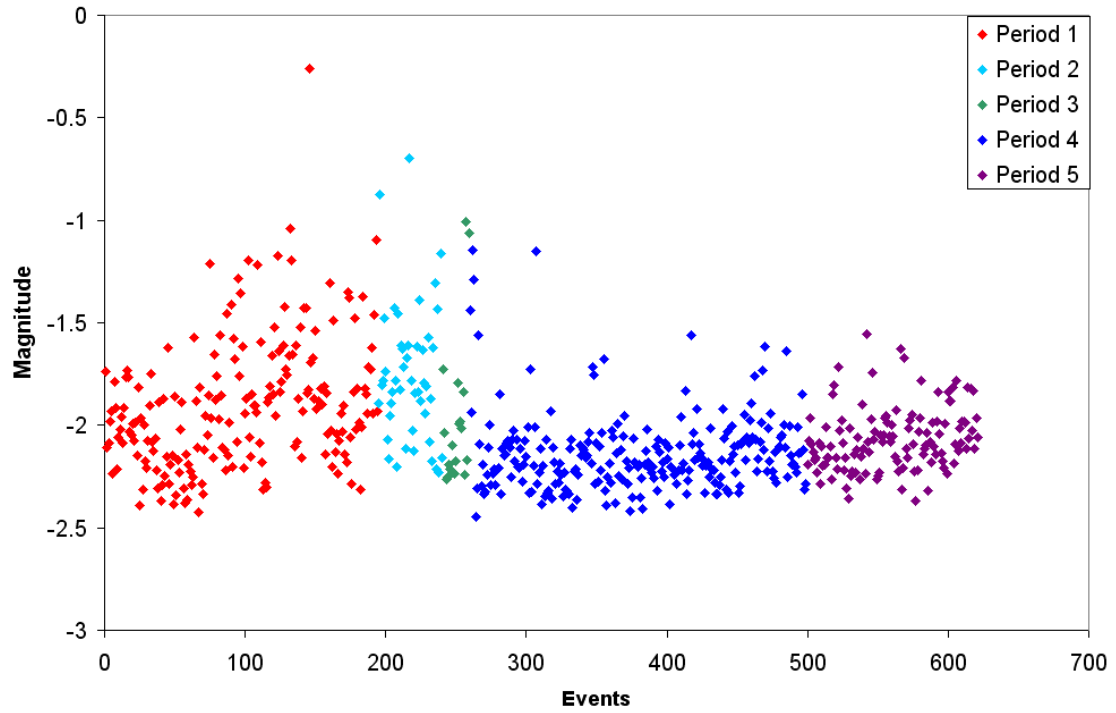
Figure 3-19: *Chart displaying AE magnitudes recorded from the beginning of heating and pressurisation. Events are coloured by period as defined in Table 4-1. Higher magnitudes were recorded during the early periods (Period 1 and 2).*

51

4   Conclusions

4.1   Monitoring Between April 2007 and September 2007

- This report describes results from acoustic emission (AE) and ultrasonic monitoring around a canister deposition hole (DA3545G01) in the Prototype Repository Experiment at SKB's Hard Rock Laboratory (HRL), Sweden. The monitoring aims to examine changes in the rock mass caused by an experimental repository environment, in particular due to thermal stresses induced from canister heating and pore pressures induced from tunnel sealing. Monitoring of this volume has previously been performed during excavation [*Pettitt et al.*, 1999], and during stages of canister heating and tunnel pressurisation [*Haycox et al.,* 2005a,b; *Haycox et al.,* 2006a,b; *Zolezzi et al.*, 2007]. This report relates to the period between 1st April 2007 and 31st September 2007, and is the fifth of an ongoing 6-monthly processing and interpretation of the results for the experiment.

- The ultrasonic velocity for each ray path is calculated initially on a 'reference survey' with an estimated uncertainty of ±30 m.s^{-1} (±3 data points). Velocity changes are measured between transmitter-receiver pairs on the daily ultrasonic surveys using a cross-correlation technique that allows a velocity resolution of ±2 m.s^{-1}. The main reason for the reduction of uncertainty when using the cross-correlation procedure is the dependency of manual picking on the user's judgement of the point of arrival. The cross-correlation procedure then allows for a high-resolution analysis to be performed and hence small changes in velocity to be observed.

- The first velocity increase is noticed between 20th and 26th April 2007 and is a similar order increase for both P- and S-waves (an average of 0.5 m.s^{-1}). The largest magnitude increase in velocity is observed on raypath transmitter 7 to receiver 6 for which P-wave velocity increases by 34.4 m.s^{-1} and S-wave velocity increases by 7.8 m.s^{-1} between 25th and 26th April 2007. A second velocity increase is observed over one day (6th May 2007) and it is particular high for P-waves (an average of 0.6 m.s^{-1}) while S-waves increase only about 0.15 m.s^{-1}. After this jump the velocities increase constantly and then on 25th June 2007 we have another sudden change. Again the jump occurs over one day and affected P-waves more than S-waves: P-waves decrease about 1.0 m.s^{-1} and S-waves 0.4 m.s^{-1}. Then velocities remain almost constant over the six month monitoring period varying by only 0.2-0.3 m.s^{-1} (see Figure 3-3).

- The increase in velocity at the end of April 2007 can be related to the increase in pressure in the backfill over the deposition hole. The magnitude of the average changes is less than the velocity resolution of 2 m.s^{-1} estimated for ultrasonic measurements, but changes on individual ray paths are significant.

- Amplitudes exhibit an increase between the 20th and 26th April. The increase for P-waves is 1.0 dB, while S-waves increase by 0.3 dB. As for velocity change, this can be related to the increase in pressure in the backfill over the deposition hole. Then the amplitudes exhibit a constant rise. P-waves increase to a greater extent, ending the monitoring period 1.5 dB greater than at the start. S-waves increase by 0.6 dB over this time.

- The P- and S-wave velocity and amplitude increases observed at the end of April 2007 are especially high for raypaths related to sensor 6, but are not restricted to that receiver. A plot of the ray-paths affected by these high variations doesn't show any particular relationship with stress regime.

- Young's Modulus and Saturation increase at the end of April and then decrease at the end of June 2007 showing the same trend for P- and S-wave velocities. Poisson's ratio show less variation in its values. Crack density shows the opposite behaviour displaying a decrease at the end of April, followed by an increase at the end of June 2007. All the ray path categories follow the same trend but the category that shows highest variation is 'Far'. These changes can be related with the rapid changes in pressure in the backfill over deposition hole DA3545G01.

- In this reporting period, 115 acoustic emissions have been located with high confidence from 221 triggered events. The rate of triggers remains reasonably constant with a maximum of six triggers recorded on one day (25th April 2007).

- Located AEs are positioned in three tight clusters labelled A, B and C. Cluster A is made up of 54 events located on the south-east side of deposition hole DA3545G01, while Cluster B (47 events) and Cluster C (14 events) are on the south-west side of the deposition hole. Clusters A and B were recognized in the previous six-months reporting period (*Zolezzi et al.*, 2007). Cluster C has not been identified previously but is located in the region of activity which occurred during excavation (*Pettitt et al.*, 2000). Events in each cluster are close enough together to be considered as occurring on the same feature. AEs may be occurring at this position due to the presence of a pre-existing structure, generated during excavation or at an intersection with a pre-exiting macrofracture. As analysed in the previous report period, no evidence of a movement of any instrument has been revealed in order to explain the presence of these clusters.

- It is important to note that events located during this reporting period are consistent with previous results, i.e. no events are positioned in regions where activity has not been observed in the past. The events can therefore be interpreted as a continuation of activity in the damage zone. We observed a minor increase in number of AEs with respect to the previous monitoring period, however the numbers of events are relatively low and therefore indicate the rock mass around the deposition holes has remained stable during this six-month period.

4.2 Summary of Monitoring from the Heating and Pressurisation Phase

- Monitoring of the heating and pressurisation phase at the Prototype Repository Experiment has been conducted since March 2003. *Haycox et al.*[2006a] present a detailed analysis of the ultrasonic measurements, and split the experiment into four periods for analysis based on environmental factors (Figure 4-1). A fifth period has been added during this report starting (14th April 2007) when an increase of P-wave and S-wave velocity and

amplitude are observed. The temperature is relativity constant from
November 2005 showing very slow increase, while the pressure is constantly
increasing. We decided to distinguish this period as it is characterized by a
gap in pressure data due to a system failure related to excavation activity on
a new tunnel near the prototype tunnel during summer and autumn 2007 and
ongoing into the next monitoring period starting 1st September 2007. Table
4-1 presents a summary of the observations from ultrasonic monitoring thus
far, and Table 4-2 provides interpretations of the rock response updated from
Haycox et al.[2006a].

- Figure 4-1 shows average P- and S-wave velocity and amplitude recorded
during the monitoring period. Figure 4-2 to Figure 4-6 provides average
velocity and modulus changes for the six ray path categories selected in
terms of disturbed and damaged regions (Figure 3-5). Figure 4-7 and Figure
4-8 show all locations and the temporal distribution of located AEs recorded
since March 2006. Figure 4-9 to Figure 4-12 summarise changes that take
place at different regions around the deposition hole in schematic diagrams
for each period, identifying the primary changes in the properties of the rock
as described in Table 4-2.

4.3   Recommendations

- The rock mass around the deposition holes has remained relatively stable during
the monitoring period and the parameters we investigate show no significant
changes, as expected when temperature and pressure remain relatively constant.
During this monitoring period a failure in the pressure monitoring system due to
excavation a new tunnel near the prototype tunnel during summer and autumn
2007 gave us a gap in pressure data. The data available show some variations in
the pressure measured in the backfill over deposition hole DA3545G01 (Figure
3-2a). These changes could be related with the variations in P- and S-waves
velocity and amplitudes (Figure 3-3). AE clusters, located with high confidence,
occur in a region of pre-existing microcracks following excavation [Pettitt et
al.,2000] and might suggest a re-activation of pre-existing fractures. The
acquisition system and instrumentation has been successfully operating at the
HRL since 2003. Ultrasonic and acoustic emission monitoring is planned to
continue for monitoring the cooling phase. The system hardware has been
operating without maintenance and is in need of upgrade as soon as is
appropriate.

- As in the previous six-months reporting period clusters of events are observed to
locate on the SW and SE walls of the deposition hole. It would be interesting to
carry out further study on these events to investigate their mechanisms of failure
and how they have changed over time, in relation to changing environmental
variables. The objective would be to resolve the primary factors responsible for
causing AEs in that particular position.

Table 4-1: Summary of velocity, amplitude and AE variation measured during four periods of temperature and/or pressure change.

Name / Date	Temperature/Pressure	Velocity	Amplitude	AE
PERIOD 1 25th May 2003 to 31st October 2004	Heaters in canister switched on causing an initially rapid change in temperature which gradually levels out to a constant increase. An increase of 35ºC is measured for an instrument in rock adjacent to the deposition hole. Pressure constant	Rapid increase in P- and S-wave velocity on 'S3' category. Other categories show increases but to a lesser extent. Initial decrease in P-wave velocity in comparison to S-wave velocity for all ray paths except for 'S3'.	Amplitudes increase over this period by between 3dB and 9dB for P-wave amplitude, and 7dB and 12dB for S-wave amplitude.	AEs do not start immediately after heating. This could be a Kaiser-type effect in which AE rate remains close to background level until stress increases above the largest previous value. Peak of 13 events located on 26th June 2003. Average Event Rate = 0.5 / day
PERIOD 2 1st November 2004 to 4th September 2005	Drainage to tunnel closed on 1st November. Pressure in tunnel increases. Pressure increases measured in the deposition-hole buffer between 3rd and 5th December. Damage observed on canister on 6th December so drainage reopened and heaters switched off. Power switched on 15th December.	Velocity increases measured close to the tunnel from 26th November. Larger increases measured on categories 'S1' and 'S3'.	Amplitude increases measured close to the tunnel from 26th November.	Relatively large number of events recorded in this period. Peak rate of 32 AEs on 4th and 5th December. Events locate in clusters in previously observed damage zone. Average Event Rate = 0.4 / day
PERIOD 3 5th September 2005 to 2nd November 2005	Additional drainage is opened in August 2005 leading to a decrease in pressure and temperature. Heaters turned off on 5th September	P- and S-wave velocities decrease on all ray path categories except 'far'.	P-wave amplitude decrease on all category ray paths.	Slight increase in event rate above background rate recorded in previous 5 months. Average Event Rate = 0.3 / day
PERIOD 4 3rd November 2005 to 13th April 2007	Pressure in tunnel increases. Constant increase in pressure in buffer above deposition hole. Heaters switched on again so temperature around deposition hole increases.	P- and S-wave velocities increase on all category ray paths. Larger increases measured on 'S3'.	P- and S-wave amplitude increase on the majority of ray paths.	Cluster of 202 events located on SE side of deposition hole. Similar rate of AE locations. Average Event Rate = 0.46 / day
PERIOD 5 14th April 2007 to 31st September 2007	Variations of pressure in tunnel. Constant increase in pressure in buffer above deposition hole. Missing pressure data period (24/06/2007-09/09/2007).	P- and S-wave velocities increase on all category ray paths. Larger increases measured on all ray paths related to instrument 6.	P- and S-wave amplitude increase on all ray paths.	115 events located in 3 different Clusters on SE and SW side of deposition hole. Similar rate of AE locations. Average Event Rate = 0.62 / day

Table 4-2: Summary of key interpretation of rock response from the ultrasonic measurements.

Period	Summary of Key Interpretations
1	The heaters are switched on. The 'S3' category passes through a volume that is unloaded and hence experiences low compressive stresses. This volume responds more rapidly to thermal stresses because existing microfractures are initially unloaded and hence more open than microfractures in the compressive region. P- and S-wave velocities decrease a similar amount during excavation as they increase during heating. This suggests very strongly that the microfractures induced in the regions of tensile damage around the deposition hole close when thermal stresses are applied. The difference in the rate of response between ray paths in the compressive categories was interpreted as a different magnitude of response of the microfractures in the rock mass to increasing thermal stresses. In the first few months of heating, another effect is superimposed onto the rock's response to thermal stresses. This is measured as a reduction in P-wave velocities compared to S-wave velocities in the first few months of heating. This is particularly noticeable on 'S1' category in Figure 4-2, in which P-wave velocity decreases by about 3.5 m.s^{-1} while S-wave velocity remains constant. A desaturation occurs on all ray path categories, other than 'S3'. This must be caused by a drying of the rock mass, in the zones experiencing high compressive stresses, as heat is applied to the rock (i.e. both temperature and pressure are acting to expel moisture). In the low-compressed, or tensile, region saturation increases during this period. This is probably caused by hot fluids expanding into the open microfracture fabric.
2	Pressure rose rapidly after drainage from the tunnel was closed. This resulted in damage to the canister and the heaters being temporarily switched off. Temperature around the deposition hole dropped rapidly, but started increasing again after 13 days. Significant changes to the character of many recorded ultrasonic waveforms were observed as significant increases in signal quality. This suggests that as pressure increased in the rock surrounding the deposition hole, attenuation of the ultrasonic waves is significantly reduced meaning that they can pass more efficiently through the rock medium. The pressure increase can be interpreted as increasing the stiffness of the rock with a corresponding decrease in crack density. The magnitude of increase is greater for 'S1' and 'S3' categories because the volumes through which they pass are close to the deposition holes and contain a higher proportion of microfractures in an excavation damage zone. The pressure increase acts as a confining pressure on the rock mass leading to a closure of the pre-existing microcrack fabric and therefore a reduction in crack density. We observe that only a relatively small pressure increase is sufficient to close this microcrack fabric in the volumes already under high compressive stresses, leading to an initially high rate of change in measured velocities followed by a constant level, even though pressures may keep increasing afterwards. From Figure 4-2 the required pressure increase is approximately 1.5MPa. The rapid pressure increase led to 32 events locating in clusters over the course of two days. The events are interpreted as stress changes in the rock as it responds to the sudden pressure change. This induces small scale movement on pre-existing microcracks, or induces new microfractures in weaker volumes of the rock. Pore pressure increases may also have assisted in inducing slip on pre-existing microfractures, by reducing the normal stress on the fractures. Over the rest of this period, as pressure continued to increase, fewer events were located. Another effect at this time is a rapid cooling of the rock when the heater inside the canister is switched off (for 13 days between 2nd and 15th December 2004), followed by warming as the rock is reheated. The majority of categories do not show a significant change in P- or S-wave velocity during this period indicating they are relatively insensitive to temperature changes at this time (i.e. when pressures are high). The exception is category 'S3', which exhibits a decrease in P- and S-wave velocity followed by an increase that mirrors the rate at which temperature changes (Figure 4-3). This category was found to be the most sensitive to thermal stresses during the initial stages of heating. When the rock cools, thermal stresses acting in this volume of low compressive (or slightly tensile) stresses reduce causing unloading of the microcracks. Microcracks close again when the rock is reheated and thermal stresses increase.

3	In September 2005 additional drainage from a permeable mat placed on the inner surface of the outer plug was opened, and heaters were switched off. This resulted in a cooling and de-pressurisation of the deposition hole. Neither temperature nor pressure reduced to the background level.
	The decrease in velocity on most ray paths is generally low compared to the increases observed previously. An exception to this is category 'S3'. This category is observed as the most sensitive. As temperature and pressure decreases, stresses again reduce in this volume causing microcracks to reopen and resulting in an increase in crack density and reduced stiffness of the rock.
	At the start of the period a sudden (over a few days), but relatively small change in velocity is observed, superimposed on the longer-term trends. We believe these are related to rapid changes in fluid pressure; a corresponding increase is observed at the end of the period (start of Period 4). For Period 3, an increase in Young's Modulus occurs which indicates a stiffening of the rock. This short term change is therefore likely to be a sudden reaction of the rock mass to the decrease in fluid pressure, perhaps caused by a general closing of microcracks caused by decreased pore pressures. The reverse is true for Period 4, when a pressure increase leads to a general opening of microcracks caused by increased pore pressures. This is believed to be a different response to long term trends from thermal stresses and general confining of the rock mass.
4	During the fourth period, heaters were turned back on once more causing temperature around the deposition hole to increase. Pressure increased rapidly again, probably caused by changes in the buffer temperature (changes in water volume caused by the temperature in combination with low hydraulic conductivity) [*Johannesson*, 2006]. Velocity increases rapidly at first, then at a constant rate, following a similar pattern to the temperature and pressure.
	Ray path category 'S3' exhibits the greatest increase in P and S-wave velocity. Similar patterns are observed on 'S1' and 'C1', and to a lesser extent on 'C2'. Velocity on the 'far' ray path category remains constant throughout the period. When temperature and pressure start to increase the stiffness of the rock increases, particularly on 'S3'. This is accompanied by a reduction in crack density. The associated increase in stiffness and decrease in crack density can be interpreted as the closing of existing microfractures and pore spaces as observed previously. This effect has continued to the current day.
	Few events have been located during Periods 3 and 4. A rapid decrease, and then increase, in pressure and temperature appears to have no significant affect on the number, or distribution of AEs around the deposition hole. The AE rate marginally increased since February 2006 (Figure 4-8). The vast majority of events locate on a single cluster in the south-east of the deposition hole and at 455.1m depth. The low number of AEs suggests the rock mass has stabilised. The high pressures result in a confining pressure being placed on the rock around the deposition hole and inhibit the movement on microcracks or macrofractures.
5	During the fifth period some activity for boring of a new tunnel near prototype tunnel during summer and autumn 2007 results in a gap in pressure data. The total pressure in the backfill over deposition hole DA3545G01 shows some changes during this reporting period. Pressure starts increasing at the start of the period. An increase of 0.4 MPa, followed by a sudden decrease of the pressure is observed on 22nd of May 2007 (the decrease is about 0.08 MPa). The following day the pressure rises again until the 2nd June 2007, when a progressive decrease in all the values is observed. We do not have any pressure values between 24th June and 9th September 2007. Temperature remains very stable over the six month monitoring period increasing by only 0.1 - 0.2 °C.
	Velocity and amplitude for both P- and S-waves increase between 20th and 24th April 2007. Following this change, amplitudes constantly increase, while velocities are affected by another increase over one day on 6th May 2007 and then a suddenly decrease on 25th June 2007. For the remaining period velocity increases constantly without any relevant changes. P-waves show higher variation than S-waves. The most sensitive ray-paths at the changes are those related with sensor 6. Analysing the different ray-paths we noticed how category 'Far' shows the maximum velocity changes for both P- and S- waves while category 'C1'shows minor changes. The minimum variation in signal amplitudes is observed for 'S3' category.
	During this monitoring period 115 events have been located with high confidence from 221 triggered events. The AE rate has been marginally increasing since February 2006 (Table 4-1), and also with respect to the previous period. All the events are located in 3 different clusters on the SE and SW side of the deposition hole, all at 455.1m depth. Thus can be interpreted as a continuation of activity in the damage zone, and could be created either by movement on pre-existing microcracks, or as a result of extension or formation of new microcracks in the existing damaged region. The low number of AEs suggests the rock mass is stable.
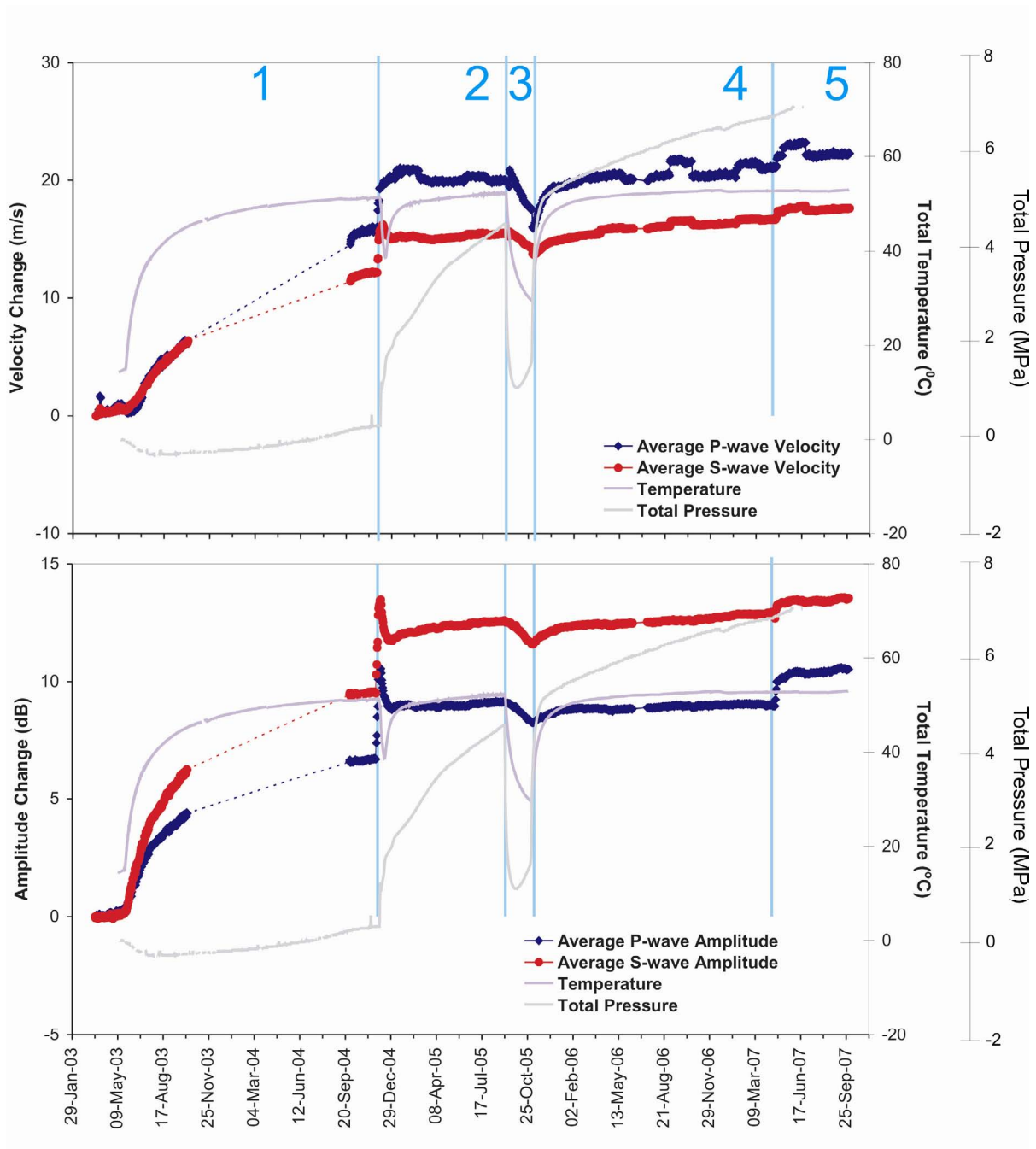
Figure 4-1: *P- and S-wave (a) velocity change and (b) amplitude change from the start of monitoring, plotted alongside temperature (TR6045) and pressure (PB616) measurements in deposition hole DA3545G01. The vertical blue lines differentiate between periods of similar environmental conditions (see Table 4-1).*
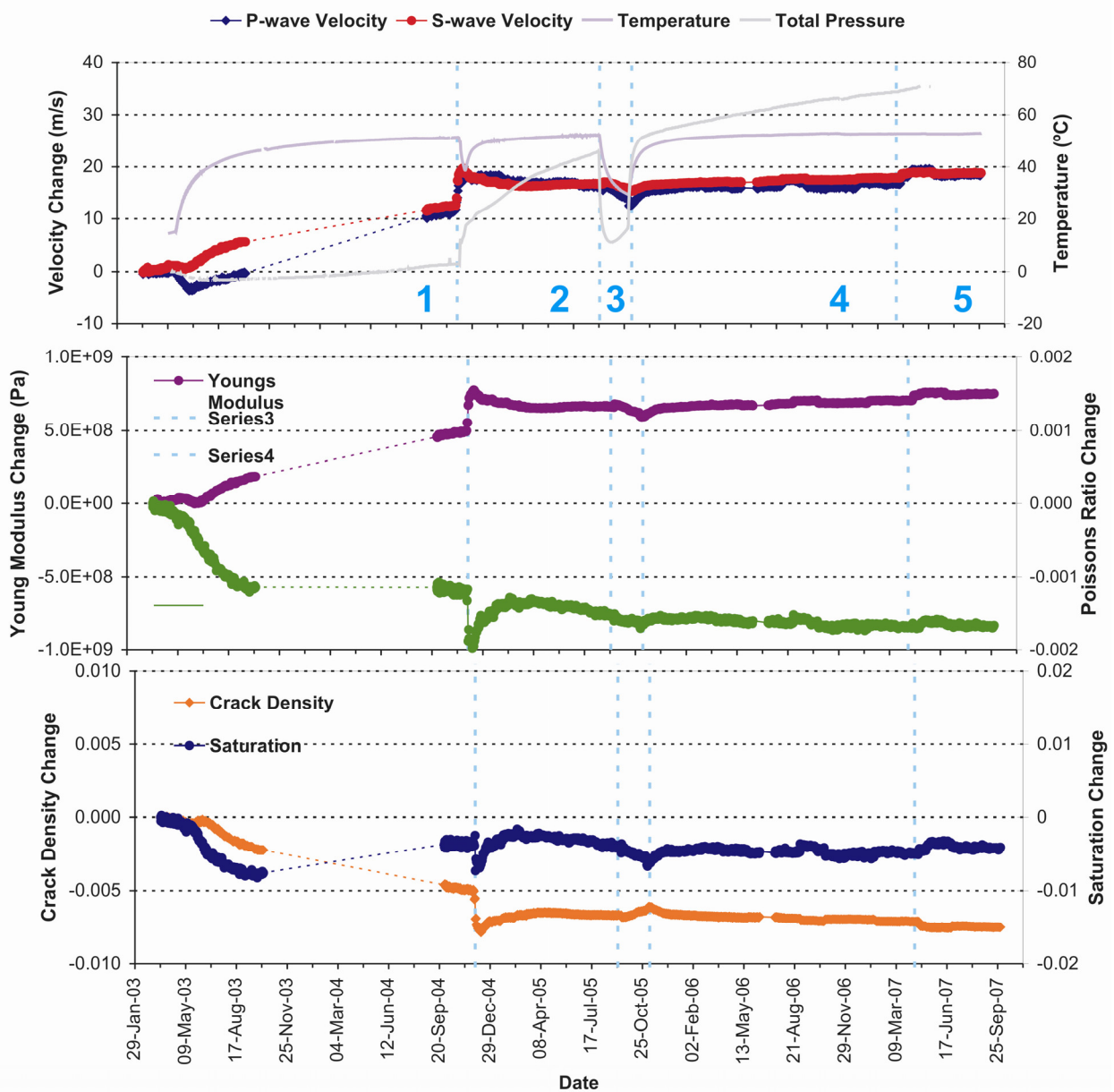
Figure 4-2: *Average P- and S-wave velocity change for ray paths on category 'S1' together with temperature (TR6045) and total pressure (PB616) (top), Young's Modulus and Poison's Ratio change (middle), and Crack Density and Saturation change (bottom).*
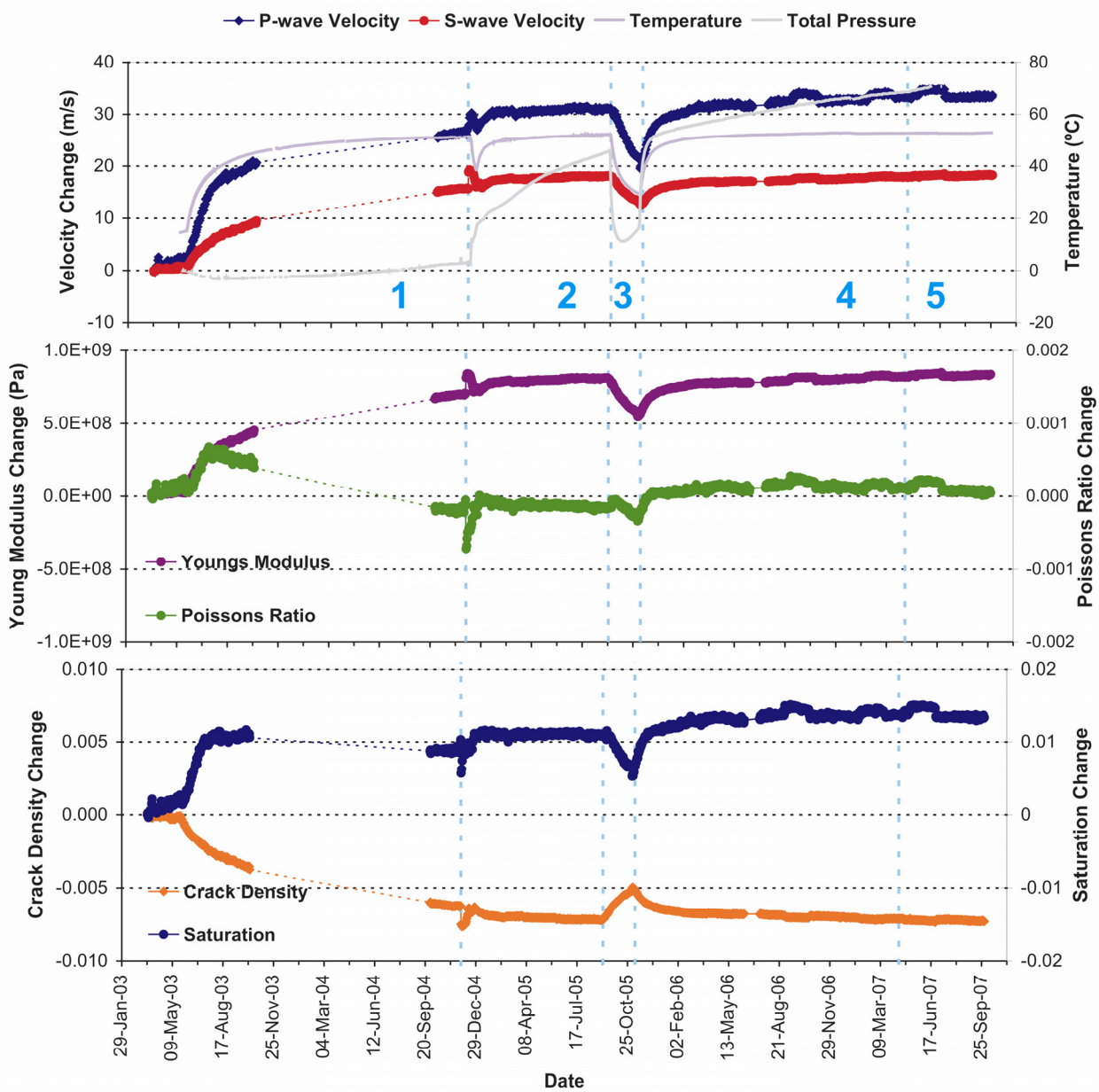
Figure 4-3: *Average P- and S-wave velocity change for ray paths on category 'S3' together with temperature (TR6045) and total pressure (PB616) (top), Young's Modulus and Poison's Ratio change (middle), and Crack Density and Saturation change (bottom).*
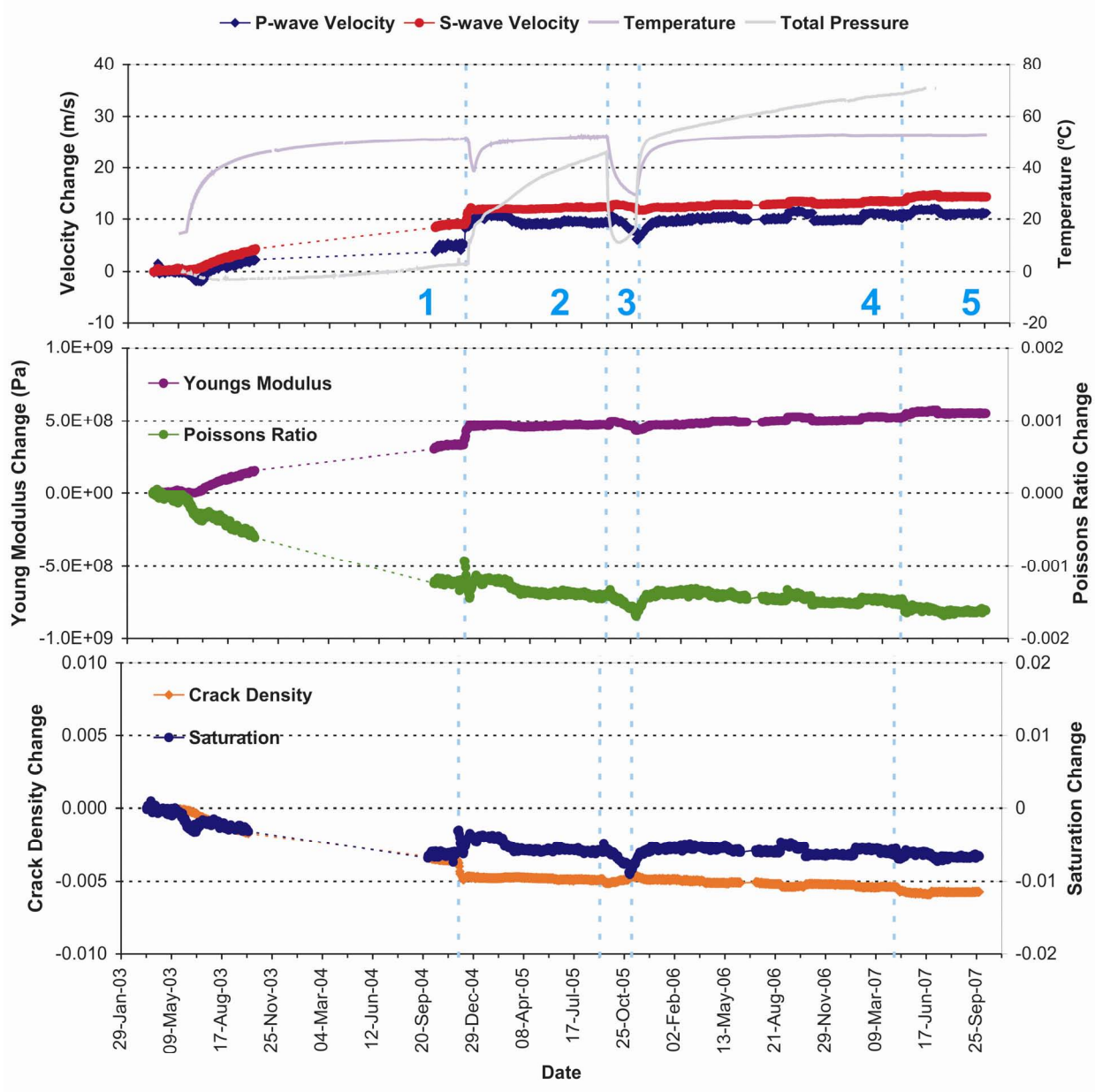
Figure 4-4: *Average P- and S-wave velocity change for ray paths on category 'C1' together with temperature (TR6045) and total pressure (PB616) (top), Young's Modulus and Poison's Ratio change (middle), and Crack Density and Saturation change (bottom).*
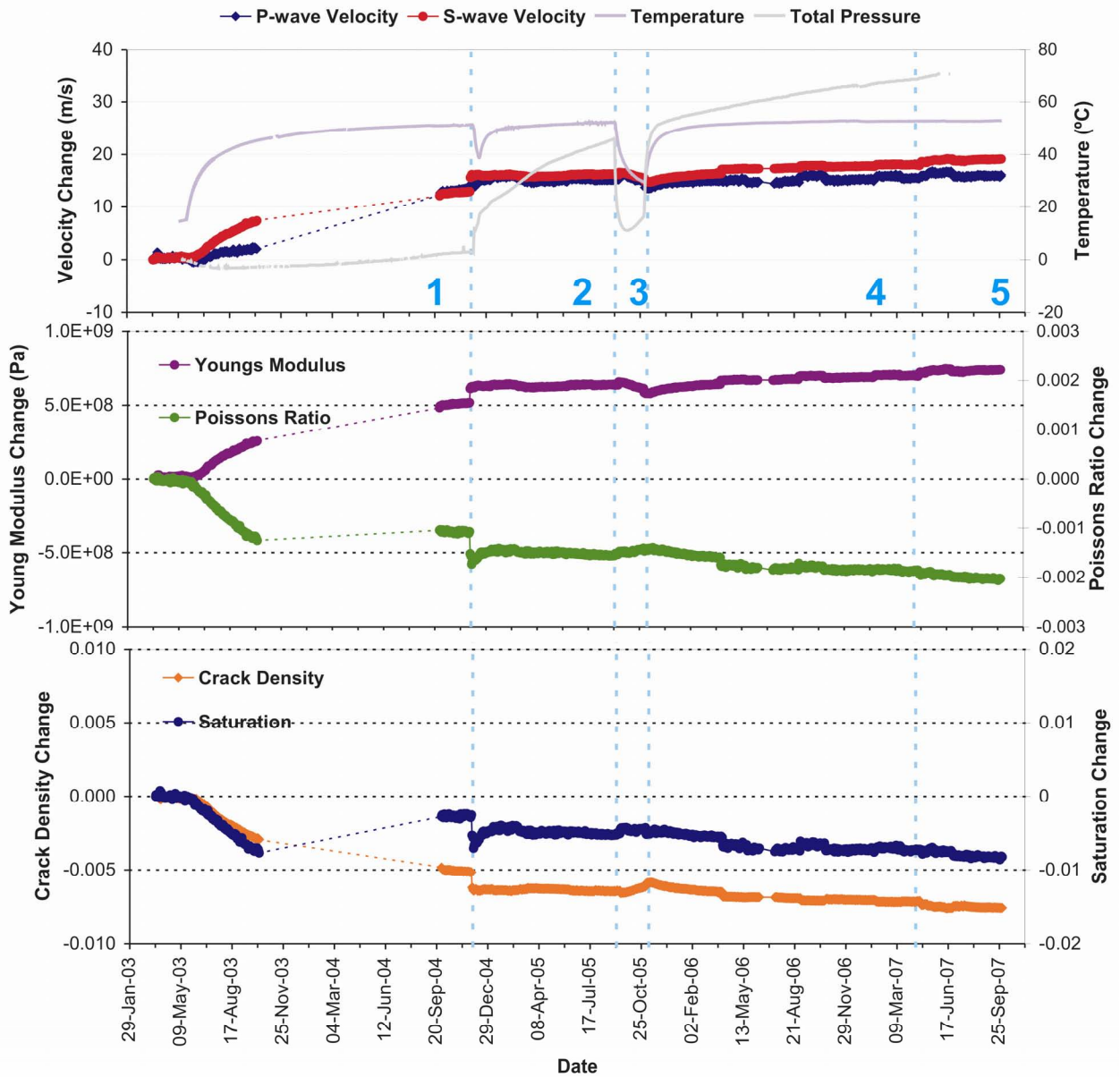
Figure 4-5: *Average P- and S-wave velocity change for ray paths on category 'C2' together with temperature (TR6045) and total pressure (PB616) (top), Young's Modulus and Poison's Ratio change (middle), and Crack Density and Saturation change (bottom).*
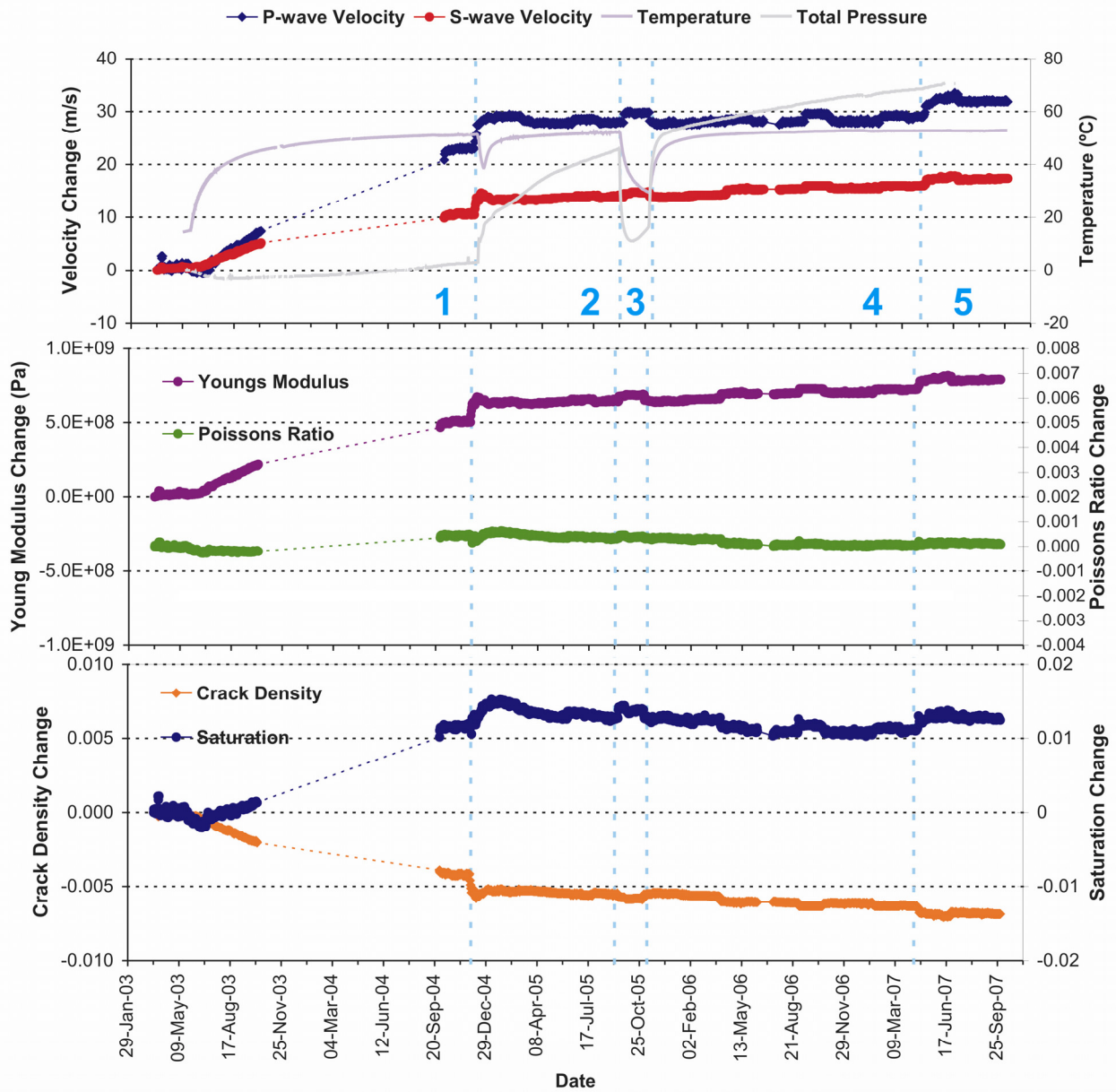
Figure 4-6: *Average P- and S-wave velocity change for ray paths on category 'Far' together with temperature (TR6045) and total pressure (PB616) (top), Young's Modulus and Poison's Ratio change (middle), and Crack Density and Saturation change (bottom).*
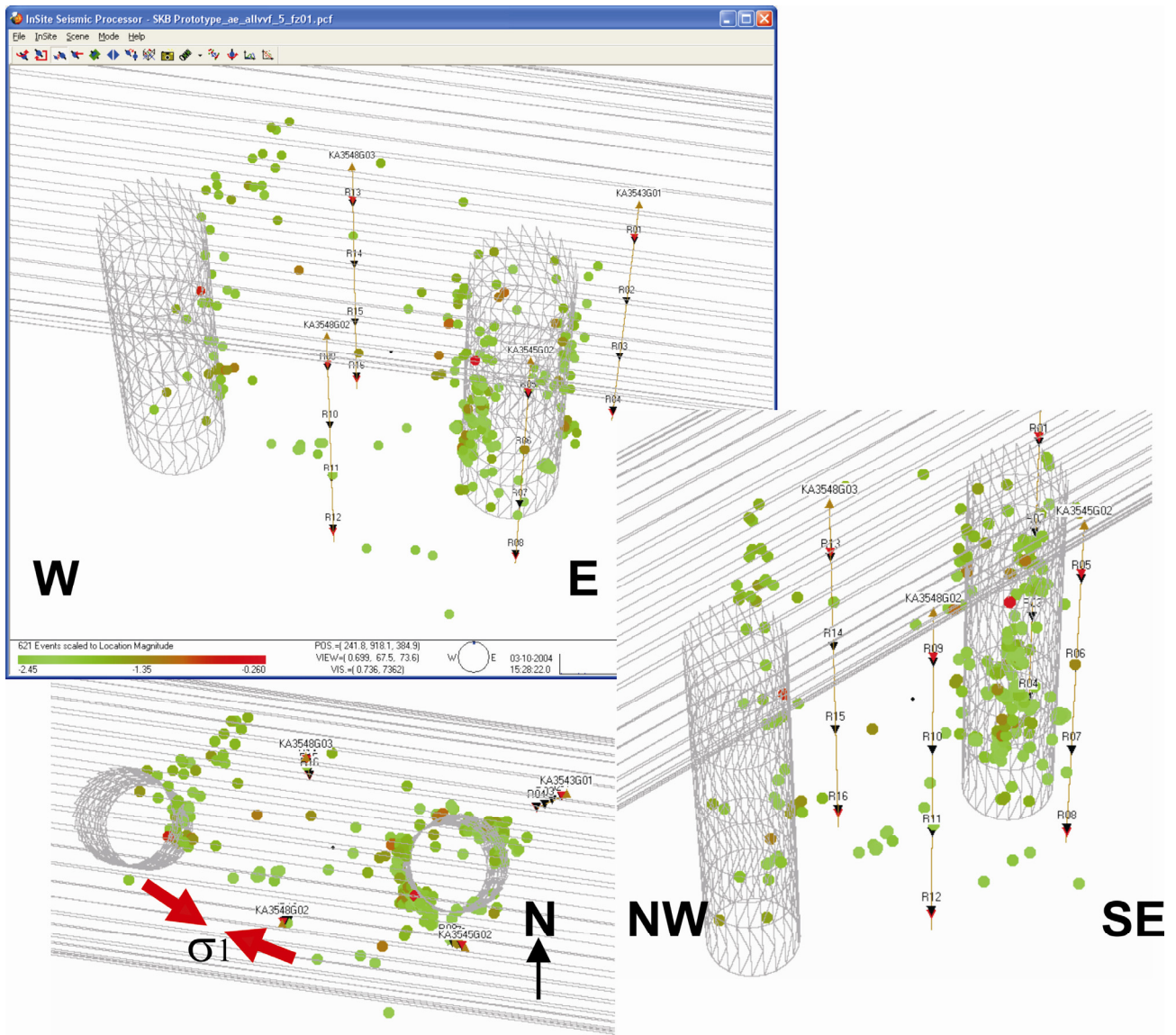
Figure 4-7: *Projections of all AEs located during the heating phase (20th March 2003 to 31st September 2007). Events are scaled to location magnitude.*
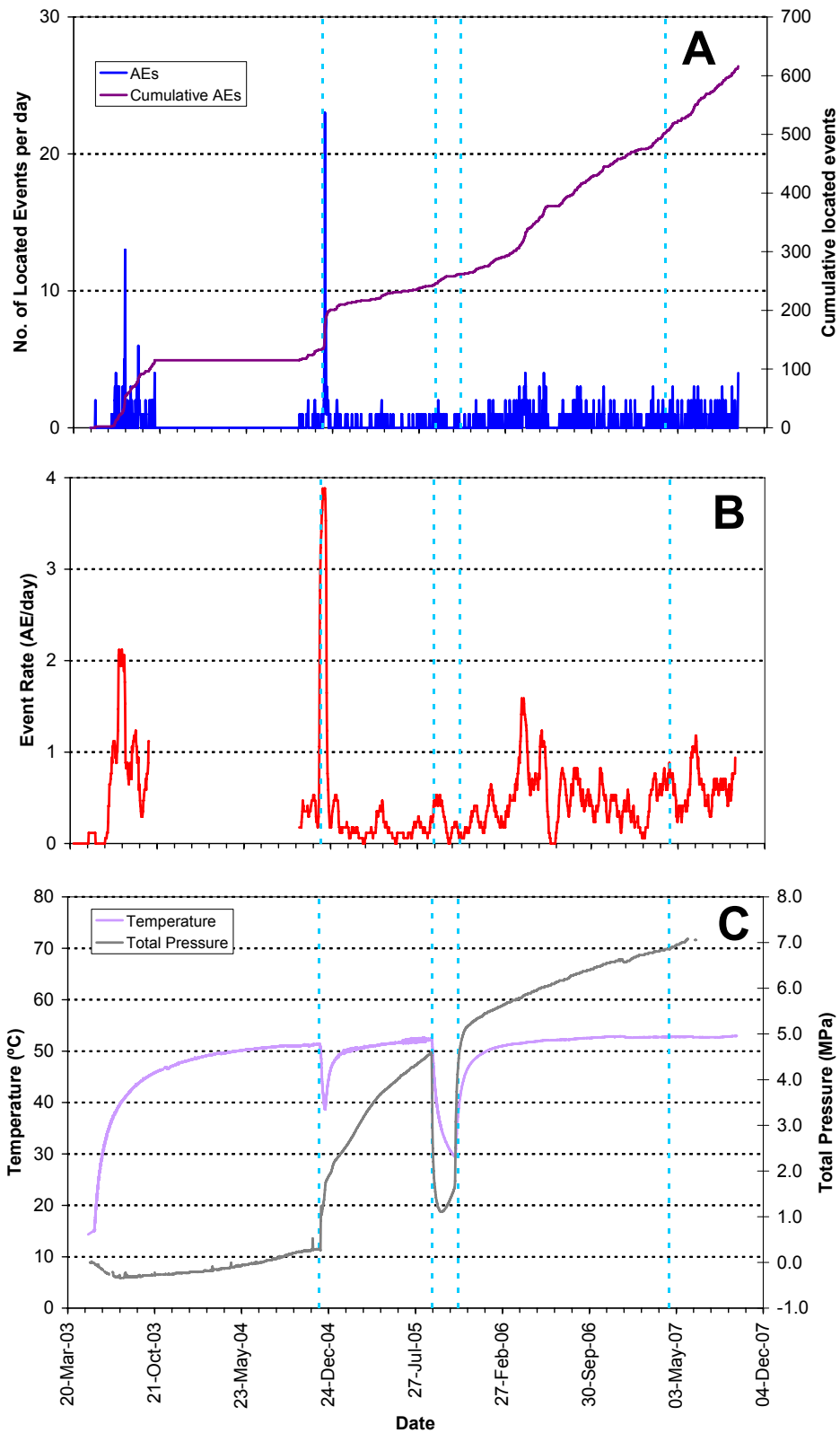
Figure 4-8: *(a) Number and cumulative number of located events from the start of monitoring, (b) average number of AE events per day (averaged over 17 days) and (c) temperature (TR6045) and pressure (PB616) measurements in deposition hole DA3545G01.*

PERIOD 1

25th May 2003 to
31st October 2004

FA

S

Rock becomes
stiffer and crack
density
reduces.Saturati
on increases.

C2

Region
desaturates and
has slight reduction
in crack density.

C1

Through
canister

S

**Temperature
increase**

**Pressure
constant**
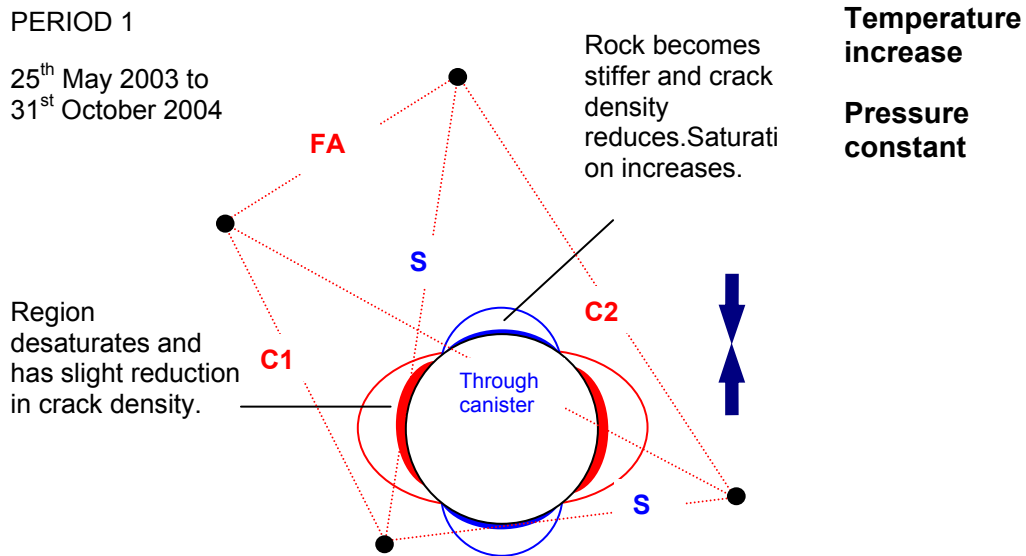
Figure 4-9: *Schematic diagram of the deposition hole and explanation of changes experienced during Period 1.*

PERIOD 21st
November 2004 to
4th September 2004

FA

S

Decrease in
crack density
and increase in
stiffness

C2

Decrease in crack
density and
increase in
stiffness

C1

Through
canister

S

**Temperature
decrease, then
increase**

**Pressure
increase**
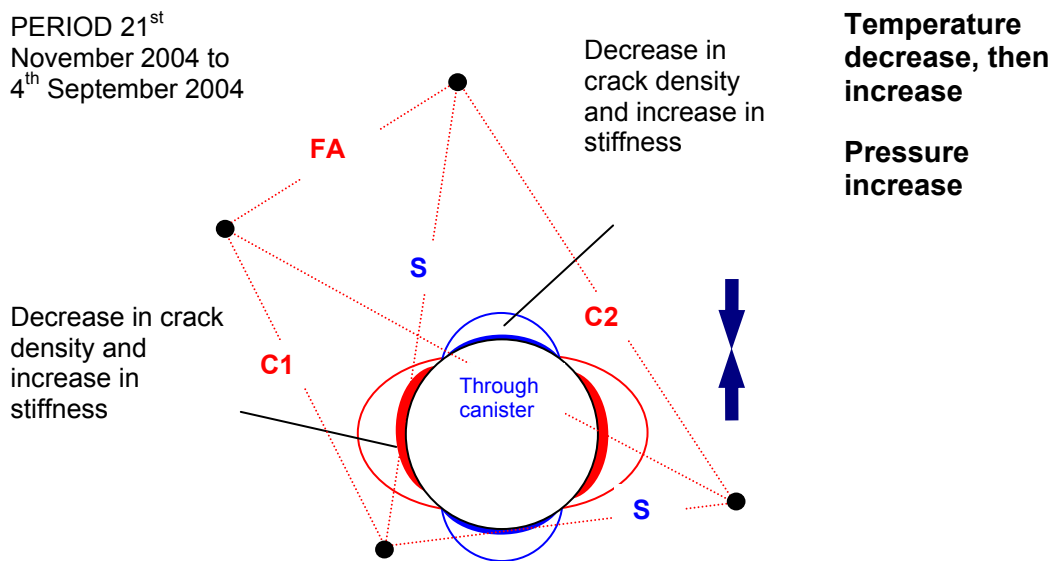
Figure 4-10: *Schematic diagram of the deposition hole and explanation of changes experienced during Period 2.*

PERIOD 3
5th September 2005 to 2nd November 2005

FA

Decrease in stiffness of this region. Crack density increases.

Decrease in stiffness of this region. Crack density increases.

S

C1

C2

Through canister

S

Temperature decrease

Pressure decrease
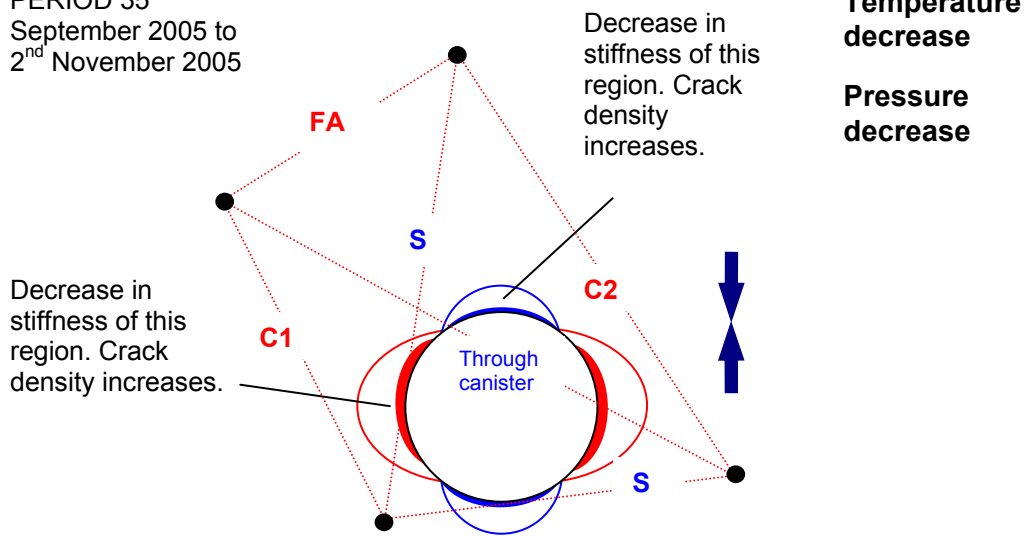
Figure 4-11: Schematic diagram of the deposition hole and explanation of changes experienced during Period 3.

PERIOD 4
3rd November 2005 to 19th April 2007

FA

Decrease in crack density and increase in stiffness.

Decrease in crack density and increase in stiffness.

S

C1

C2

Through canister

S

Temperature increase

Pressure increase
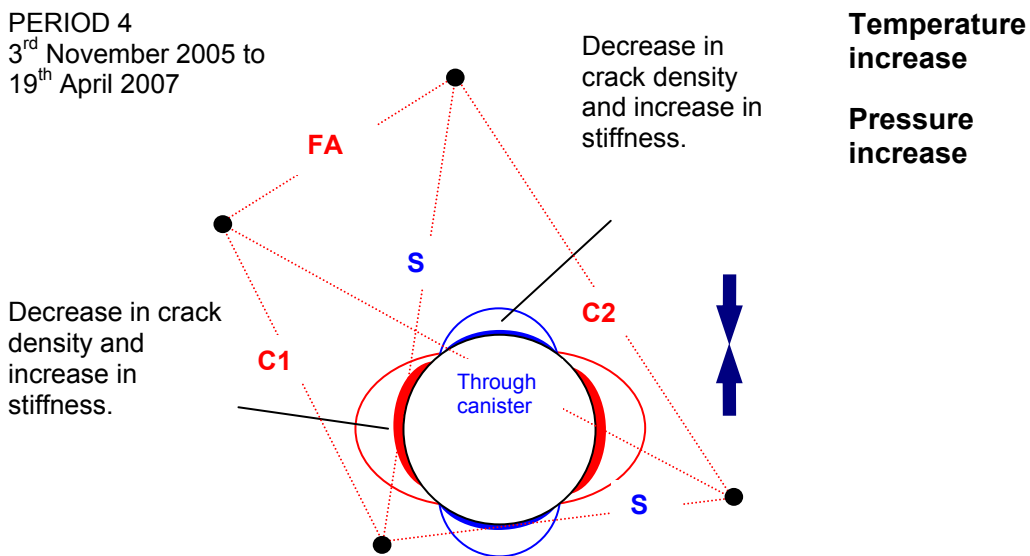
Figure 4-12: Schematic diagram of the deposition hole and explanation of changes experienced during Period 4.

References

Baker, C. and R.P. Young. 2002. Acoustic emission and ultrasonic monitoring around the TSX tunnel clay and concrete bulkheads between October 2001 and October 2002. Ontario Power Generation, Nuclear Waste Management Division Report.

Goudarzi, R. and L-E. Johannesson, Sensor Data Report (Period: 010917-061201). Prototype Repository. Report No: 16, International Progress Report IPR-07-05, Äspö Hard Rock Laboratory, Swedish Nuclear Fuel and Waste Management Company, Sweden, 2006.

Goudarzi, R., 2007. Pers. Comm.

Goudarzi, R., 2008. Pers. Comm.

Haycox, J.R., W.S. Pettitt, and R.P. Young, Acoustic Emission and Ultrasonic Monitoring During the Heating of Deposition hole DA3545G01 in the Prototype Repository to March 2005, International Progress Report IPR-05-30, Äspö Hard Rock Laboratory, Swedish Nuclear Fuel and Waste Management Company, Sweden, 2005a.

Haycox, J.R., W.S. Pettitt, and R.P. Young, Acoustic Emission and Ultrasonic Monitoring Results from Deposition Hole DA3545G01 in the Prototype Repository between April 2005 and September 2005, International Progress Report IPR-05-31, Äspö Hard Rock Laboratory, Swedish Nuclear Fuel and Waste Management Company, Sweden, 2005b.

Haycox, J.R., W.S. Pettitt, and R.P. Young, Acoustic Emission and Ultrasonic Monitoring Results from Deposition Hole DA3545G01 in the Prototype Repository between October 2005 and March 2006, International Progress Report IPR-06-23, Äspö Hard Rock Laboratory, Swedish Nuclear Fuel and Waste Management Company, Sweden, 2006a.

Haycox, J.R., W.S. Pettitt, and R.P. Young, Acoustic Emission and Ultrasonic Monitoring Results from Deposition Hole DA3545G01 in the Prototype Repository between April 2006 and September 2006, International Progress Report IPR-06-36, Äspö Hard Rock Laboratory, Swedish Nuclear Fuel and Waste Management Company, Sweden, 2006b.

Maxwell, S.C., and R.P. Young, A controlled in-situ investigation of the relationship between stress, velocity and induced seismicity, Geophys. Res. Lett., 22, 1049-1052, 1995.

Patel, S., L.-O. Dahlstrom, and L. Stenberg, Characterisation of the Rock Mass in the Prototype Repository at Äspö HRL Stage 1, Äspö Hard Rock Laboratory Progress Report HRL-97-24, Swedish Nuclear Fuel and Waste Management Company, Sweden, 1997.

Pettitt, W.S., C. Baker, and R.P. Young, Acoustic emission and ultrasonic monitoring during the excavation of deposition holes in the Prototype Repository, International Progress Report IPR-01-01, Äspö Hard Rock Laboratory, Swedish Nuclear Fuel and Waste Management Company, Sweden, 1999.

Pettitt, W.S., C. Baker, and R.P. Young, Analysis of the in-situ principal stress field at the HRL using acoustic emission data, International Progress Report IPR-01-09, Äspö Hard Rock Laboratory, Swedish Nuclear Fuel and Waste Management Company, Sweden, 2000.

Pettitt, W.S., C. Baker, R.P. Young, L. Dahlstrom, and G. Ramqvist, The assessment of Damage Around Critical Engineering Structures Using Induced Seismicity and Ultrasonic Techniques, Pure and Applied Geophysics, 159, 179-195, 2002.

Pettitt, W.S., D.S. Collins, M.W. Hildyard, R.P. Young, C. Balland and P. Bigarré. 2004. An Ultrasonic Tool for Examining the Excavation Damaged Zone around Radioactive Waste Repositories – The OMNIBUS project, in *EC Euradwaste04 Conference*, Luxembourg.

Pettitt, W.S., Baker, C., Collins, D.S., and R.P. Young, 2005. InSite Seismic Processor – User Operations Manual Version 2.13. Applied Seismology Consultants Ltd., Shrewsbury, UK.

SKB, Äspö Hard Rock Laboratory: Current Research Projects 1998, Swedish Nuclear Fuel and Waste Management Company, Sweden, 1999.

Telford, W.M., Geldart, L.P., and Sheriff, R.E., Applied Geophysics: Second Edition, Cambridge University Press, 1990.

Young, R.P. and W.S. Pettitt, Investigating the stability of engineered structures using acoustic validation of numerical models, in Geotechnical Special Publication No 102, edited by J.F. Labuz, S.D. Glaser, and E. Dawson, pp. 1-15, ASCE, USA, 2000.

Zimmerman, R.W and M.S. King, Propagation of acoustic waves through cracked rock, 20th Symposium on Rock Mechanics, Rapid City, SD, 1985.

Zolezzi F., Haycox J. R. And Pettitt W. P., Acoustic Emission and Ultrasonic Monitoring Results from Deposition Hole DA3545G01 in the Prototype Repository between October 2006 and March 2007, International Progress Report IPR-06-23, Äspö Hard Rock Laboratory, Swedish Nuclear Fuel and Waste Management Company, Sweden, 2007.

Appendix I   Previous Monitoring at the Prototype Repository

Ultrasonic monitoring has been conducted at the Prototype Repository in some form since September 1999. During excavation, monitoring of both deposition holes in Tunnel Section 2 (DA3551G01 and DA3545G01) was undertaken to delineate zones of stress related fracturing and quantitatively measure fracturing in the damaged zone [*Pettitt et al.*, 1999]. Thereafter, monitoring has been undertaken on a single deposition hole (DA3545G01), and the response of the surrounding rock to changes in temperature and pressure has been measured (see Figure 4-3). The report, by *Haycox et al.*[2006a], was the first of an ongoing 6-monthly processing and interpretation of the results, which continued the following six months by the report *Haycox et al.*[2006b]. This report presents new results from the period 1st October 2006 to 31st March 2007.

Table 4-3: Summary of ultrasonic monitoring at the Prototype Repository to-date. Response Periods are defined in Haycox et al.[2006a].

Report	Monitoring Period	Location	Response Period
Pettitt et al.[1999]	25/08/1999 to 18/09/1999	DA3551G01 and DA3545G01	Excavation
Haycox et al.[2005a]	20/03/2003 to 09/10/2003	DA3545G01	1
	29/04/2004 to 31/03/2005	DA3545G01	1, 2
Haycox et al.[2005b]	01/04/2005 to 30/09/2005	DA3545G01	2, 3
Haycox et al.[2006a]	01/10/2005 to 31/03/2006	DA3545G01	3, 4
Haycox et al.[2006b]	01/04/2006 to 30/09/2006	DA3545G01	4
Zolezzi et al.[2007]	01/10/2006 to 31/03/2007	DA3545G01	4
Zolezzi et al.[2008]	01/04/2007 to 31/09/2007	DA3545G01	4,5

A temporary ultrasonic array was installed around the rock volume when deposition hole DA3545G01 and its neighbour DA3551G01 were first excavated in September 1999 [*Pettitt et al.*, 1999]. A total of 2467 AE triggers were obtained during monitoring of the two deposition holes. Of these 1153 were located. There was significantly more AE activity around the second deposition hole (labelled DA3545G01) than the first (DA3551G01). This difference is likely to depend upon intersection of the excavation with a greater number of pre-existing fractures. These fractures may be preferentially located in the side wall of the deposition hole or preferentially orientated to the *in situ* stress field. Fracturing associated with excavation-induced stresses was observed with AEs distributed mainly in regions orthogonal to the maximum principal stress, σ_1. This was consistent with observations from the Canister Retrieval Tunnel and from dynamic

numerical models. AEs, and hence microcrack damage, were shown to locate in clusters down the deposition hole and not as a continuous 'thin skin'. *Pettitt et al.*[2000] showed that these clusters were associated with weaknesses in the rock mass generated by excavation through pre-existing fractures. Damage in the side wall of the deposition holes depended significantly on these pre-existing features. The *in situ* stress field was a contributing factor in that induced stresses were sufficiently high to create damage in these weakened regions although not sufficiently high to create significant damage in the rock mass as a whole.

A permanent ultrasonic array, with transducers grouted into instrumentation boreholes, was installed in the rock mass in June 2002. In this arrangement, ultrasonic monitoring has been conducted between 20th March and 9th October 2003, and then from 29th September 2004 to the present. A gap in monitoring occurred when the ultrasonic acquisition system was used for another experiment in the HRL (Pillar Stability Experiment). Processing and reporting of results has been undertaken by *Haycox et al.*[2005a], *Haycox et al.*[2005b], *Haycox et al.*[2006a] and *Haycox et al.*[2006b] and is further discussed in Section 4.2. A description of instruments measuring other environmental factors (such as temperature and pressure) and their locations can be found in *Goudarzi and Johannesson*[2007].

Appendix II   Methodology

Data Acquisition

The ultrasonic array consists of twenty-four ultrasonic transducers configured as eight transmitters and sixteen receivers installed into four instrumentation boreholes. The transducers are fixed into the boreholes using specially designed frames (Figure 4-13) – two transmitters and four receivers per frame. The boreholes are vertical, 76mm in diameter and approximately 10 meters in length distributed around each deposition hole volume. The array has been designed so as to provide good coverage for AE locations and to provide 'skimming' ray paths that pass within a few centimetres of the deposition-hole void so as to sample the rock immediately adjacent to the deposition-hole wall. The layout of the instrumentation boreholes is shown in Figure 4-13 and described further in Table 4-4. Each of the ultrasonic transducers has a hemispherical brass cap fixed over its active face and is then spring-loaded against the borehole surface so as to obtain good coupling to the rock mass. The boreholes have then been filled with a slightly expansive grout so as to permanently fix the transducers in place, reduce the likelihood of damage to the transducers and to remove the borehole voids.

Figure 4-13: *Top: Schematic diagram of the locations of all transducers on a single frame. Left: Photo of a section of the transducer assembly. Right: The transducer assembly during installation.*

The piezoelectric transducers operate by converting a transient elastic wave into an electric signal or visa versa. The monitoring system is then operated in one of two modes. The first is used to passively monitor AE activity preferentially within the array volume. AEs release elastic energy in the same way as 'earthquakes' but over a very small scale. At these frequencies AEs have a moment magnitude (M_w) of approximately -6. They occur either during the creation process of new fractures within the medium, or on pre-existing fractures due to small scale movements. Each receiver has a frequency response of approximately 35-350kHz and contains a 40dB pre-amplifier. This minimises a reduction in signal-to-noise between the sensors and the acquisition system. The sensors have a vulcanised surround and a high pressure reinforced cable to protect them from water infiltration. In addition, polyamide tubes and *Swagelok* connectors have been fitted to the cables to reduce the likelihood of breakage.

Figure 4-13 shows a schematic diagram of the acquisition system used. Cables from each transducer pass through the pillar between the PRT and the G-tunnel. Data acquisition uses a Hyperion Ultrasonic System controlled by a PC, set up within a cabin provided by SKB. This has 16 receiving channels and 8 transmitting channels. An AE is recorded when the amplitude of the signal on a specified number of channels exceeds a trigger threshold within a time window of 5ms. The system then records the full-waveform signals from all 16 transducers. In this case a trigger threshold of 50mV on three channels was used. This allows the system to have sufficient sensitivity to record high quality data without recording an abundance of activity that cannot be processed due to very small signal to noise on only a few channels. The captured signals are digitised with a sampling interval of 1μs and a total length of 4096 data points. In general, low noise levels were observed (<2mV) giving high signal to noise and good quality data. AE monitoring is set to switch off during daytime working hours (6am-8pm) so as to minimise the amount of noise recorded from human activity.

A second operating mode actively acquires ultrasonic waveforms by scanning across the volume. This allows measurements of P- and S-wave velocities and signal amplitudes over a possible 128 different ray paths. By repeating these ultrasonic surveys at increments in time, a temporal analysis is obtained for the variation in medium properties. Ultrasonic surveys are conducted daily at 1am in order to measure changes in P- and S-wave signals. At that time of night, no human activity will cause noise that can interfere with the signals received. A Panametrics signal generator is used to produce a high frequency electric spike. This is sent to each of the 8 transmitters in turn. The signal emitted from each transmitter is recorded over the 16 receivers in a similar fashion to that described above. An external trigger pulse from the signal generator is used to trigger the acquisition system and identifies the transmission start time to an accuracy of one sample point. In order to decrease random noise the signal from each transmitter is stacked 100 times.

Table 4-4: Boreholes used for AE monitoring of deposition hole DA3545G01.

SKB Borehole designation	ASC Borehole reference	Transducer Numbers
KA3543G01	1	T1, T2, R1-R4
KA3545G02	2	T3, T4, R5-R8
KA3548G03	3	T5, T6, R9-R12
KA3548G02	4	T7, T8, R13-R16
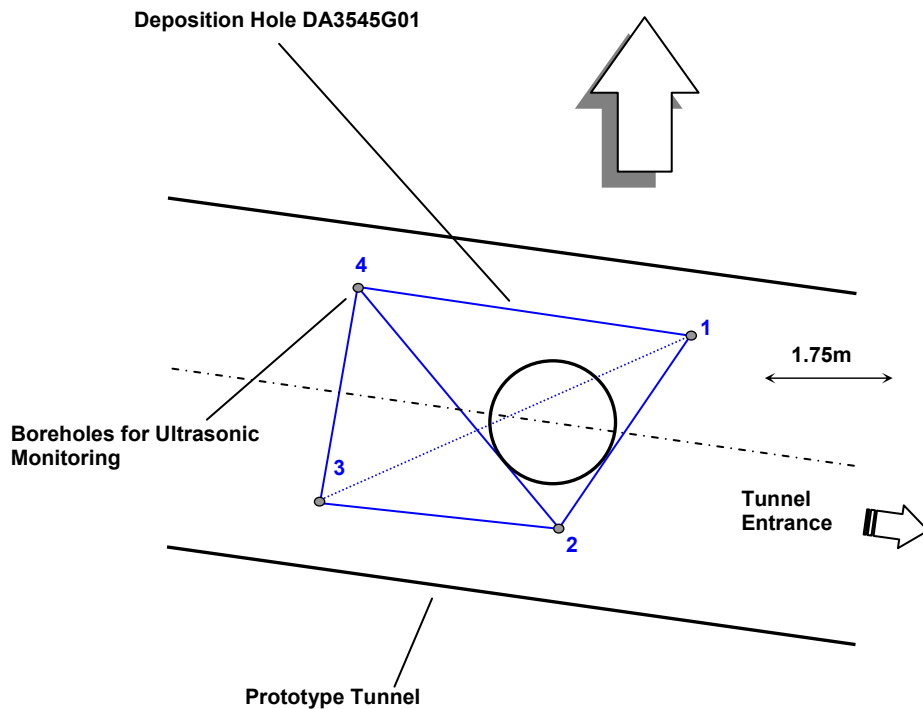
Figure 4-14: *Plan view of the array geometry for Deposition Hole DA3545G01 during heating in the Prototype Tunnel. The blue solid lines represent direct ray paths between sondes illustrating their 'skimming' nature. The blue dashed line represents a ray path that travels through the deposition hole.*
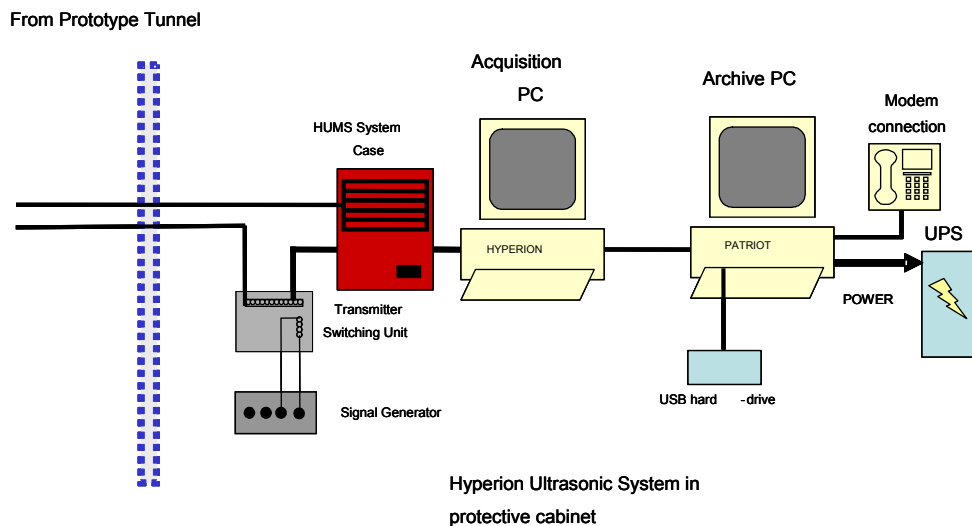
Figure 4-15: *Schematic diagram of the hardware used for the heating stage in the Prototype Repository. The ultrasonic pulse generator sends a signal to each transmitter and the resulting signal is recorded on each receiver. The receivers are also used to listen for AE activity. The archive PC is required to make a copy of the data for backup purposes.*

Processing Procedure

Overview

ASC's InSite Seismic Processor has been used to automatically process both the AE and ultrasonic survey data. Appendix IIIA and Appendix IIIB give the processing parameters used. *Pettitt et al.*[2005] provides a detailed description of this software.

Ultrasonic Data Procedure

The ultrasonic survey full-waveform data was initially stored with the AE data. This was automatically sorted and the survey data extracted to a separate processing project. A 'reference' survey from the previous monitoring period was used, and imported into the project. The P- and S-wave arrivals were manually picked during the previous monitoring period. Knowing the transmitter and receiver locations, the ultrasonic velocity for each ray path was calculated with an estimated uncertainty of $\pm 30 \text{m.s}^{-1}$ (± 3 data points). A cross-correlation procedure was then used to automatically process subsequent surveys. This technique cross-correlates P- and S-wave arrivals from a transmitter-receiver pair with arrivals recorded on the same transmitter-receiver pair on the reference survey. This results in high-precision measurements of P- and S-wave velocity change with estimated uncertainties of $\pm 2 \text{m.s}^{-1}$ between surveys. Note that when the transmitter and receiver are on the same borehole, the ray path is not used due to the introduction of transmission effects from the instrumentation borehole, grout and transducer frames.

The main reason for the reduction of uncertainty when using the cross-correlation procedure is the dependency of manual picking on the user's judgement of the point of arrival. This can usually be quite indiscriminate because of random noise superimposed on the first few data points of the first break. Additionally, the procedure is run automatically without any loss of precision resulting in efficient waveform processing. The cross-correlation procedure then allows for a high-resolution analysis to be performed and hence small changes in velocity to be observed. This is extremely important when changes in rock properties occur over only a small section (5%) of the ray path.

Figure 4-16 gives example waveforms recorded from one of the transmitters during this reporting period. Each waveform is first automatically picked to obtain an estimate of the P-wave or S-wave arrival. A window is then automatically defined around the arrival and a bell function is applied, centred on the automatic pick. The data at the ends of the window then have a much smaller effect on the cross-correlation. The windowed data is then cross-correlated [*Telford et al.*, 1990] with a similar window constructed around the arrival on the reference survey. The change in arrival time is then converted to a change in velocity knowing the manually-picked arrival time for the reference survey. Waveforms that do not provide automatic picks are not cross-correlated. This gives an automatic discrimination of signals that have very poor signal to noise ratios and could give spurious cross-correlation results from poor discrimination of the first arrival. During the automatic processing an arrival amplitude is also calculated from within a processing window defined by a minimum and maximum transmission velocity. This provides a robust measure of arrival amplitudes between surveys.
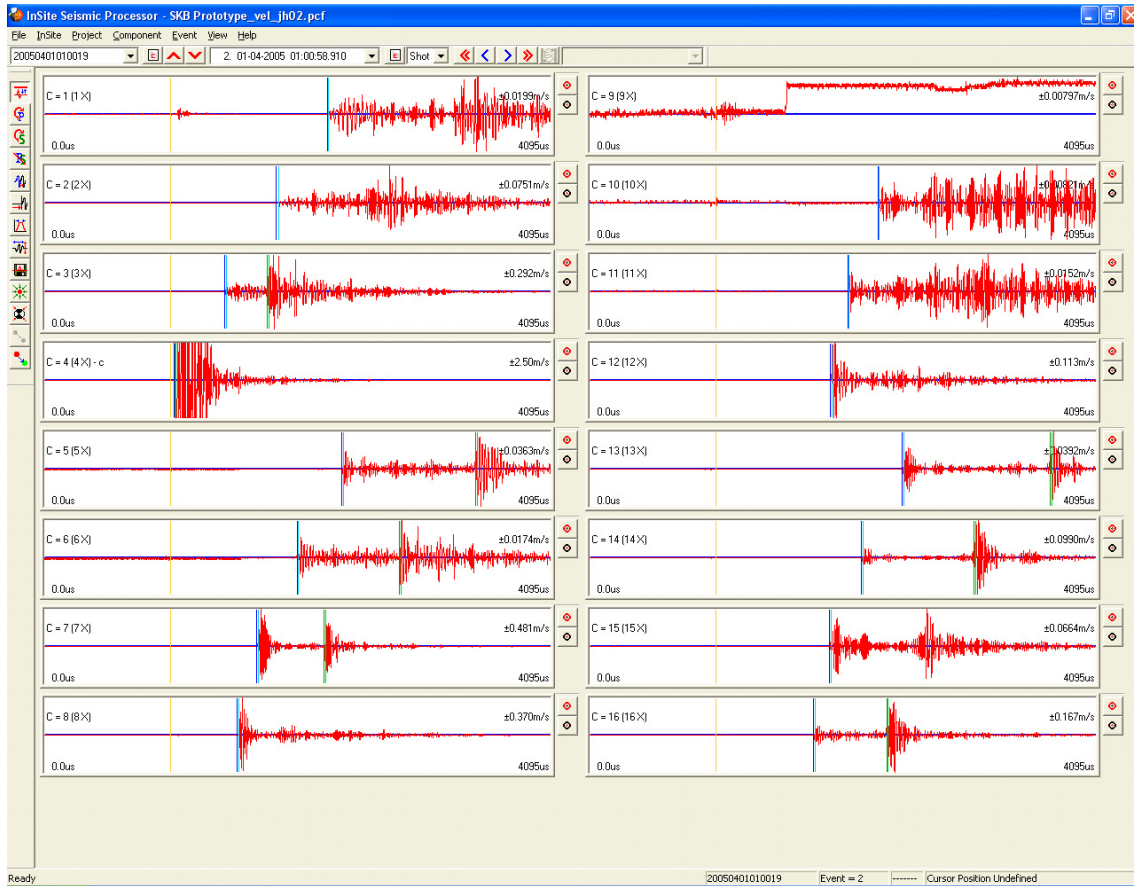
Figure 4-16: Waveforms recorded from one transmitter on the array of sixteen receivers. The gold markers indicate the transmission time. The blue and green markers indicate picked P- and S-wave arrivals respectively.

When calculating average velocities and amplitudes, ray paths passing through the deposition hole are removed due to the uncertain transmission paths produced by the wave travelling in the rock around the deposition hole and through the bentonite, fluid and canister fill. Therefore the majority of ray paths between boreholes 1 and 3 (transmitters 1, 2, 5, 6 and receivers 1, 2, 3, 4) are not used in the analysis. An exception is made for the deepest ray paths that pass under the deposition hole entirely through rock.

The dynamic Young's modulus *E*, and dynamic Poisson's Ratio, *v*, can be calculated from the velocity measurements using Equation 1 and Equation 2

$$E = \rho V_S^{\ 2} \left(\frac{3V_P^{\ 2} - 4V_S^{\ 2}}{V_P^{\ 2} - V_S^{\ 2}} \right)$$

Equation 1

$$v = \frac{V_P^{\ 2} - 2V_S^{\ 2}}{2\left(V_P^{\ 2} - V_S^{\ 2}\right)}$$

Equation 2

V_P and V_S values are also used to model for crack density (c) and saturation (s) in the rock mass using the method of *Zimmerman and King*[1985]. The crack density parameter is defined by the number of cracks (penny-shaped) per unit volume multiplied by the mean value of the cube of the crack radius (Equation 3). This method assumes the elastic modulus E and v in the damaged material normalized to the undisturbed material, decrease exponentially with crack density. Also assumed are the shear modulus (μ) is unaffected by s, and the bulk modulus (k) increases linearly with s, equalling that of uncracked rock when s=1. Equation 4 shows the calculation used to determine saturation.

$$c = \frac{9}{16} \ln\left(\frac{2\mu}{E_0 - 2\mu v_0} \right)$$ Equation 3

$$s = \frac{k(c,s) - k(c,0)}{k_0 - k(c,0)}$$ Equation 4

The calculations require an estimation of the completely undisturbed rock (i.e. an unsaturated, uncracked, intact rock mass). This study assumes values of V_{0P} = 6660m.s^{-1}, and V_{0S} = 3840m.s^{-1} for the undisturbed material taken from laboratory tests on a similar granite, summarized in *Maxwell and Young*[1995]. A value of 2650 kg m^{-3} is presented by *Pettitt et al.*[2002] for the density of the rock mass.

The calculations of Young's Modulus and Poisson's ratio from measured velocities makes an assumption of an isotropic elastic medium. Under this assumption a rock can be completely characterised by two independent constants. One case of an isotropic elastic medium is a rock with a random distribution of cracks embedded in an isotropic mineral matrix. Under the application of a hydrostatic compressive stress, the rock will stay isotropic but become stiffer (which will become characterised by increased velocity V_P, V_S and therefore increased Young's modulus). In contrast, under the application of a uniaxial compressive stress, cracks with normals parallel or nearly parallel to the applied stress will preferentially close and the rock will take on a transversely isotropic symmetry. Under this situation P- and S-wave velocities become variable with orientation. The crack density and saturation calculations also assume an isotropic elastic medium.

It should be noted that E and v calculated in this report are dynamic measurements due to the small strains exerted on the rockmass at high frequencies from the passing ultrasonic waves. Static E and v measurements, made from uniaxial laboratory tests on rock samples, may be different from dynamic values – even if sample disturbance is minimal – due to the larger strains exerted over relatively long periods of time.

Acoustic Emission Procedure

The procedure used to process the AEs in this reporting period has been undertaken as follows:

1. Calibration surveys from the installation phase (when the deposition hole was open) have been used to optimise an automatic picking and source location algorithm and check location uncertainties. ASC's InSite seismic processing software was used for location and visualisation.

2. Where possible, P- and S-wave arrival times were measured for each AE using the automatic picking procedure.

3. AEs with ≥6 P-wave arrival times were input into a downhill-simplex location algorithm [*Pettitt et al.*, 2005]. This has the option of incorporating either a three-dimensional anisotropic velocity structure or an isotropic structure. Velocities calculated from the ultrasonic surveys were used.

4. The waveforms from all events were visually inspected to ensure they were 'real' acoustic emissions. Events were removed if they had the appearance of noise spikes (increase in amplitude is recorded on all channels at the same time) or they were the result of human noise (long period events that occur at close intervals during the day).

5. The acoustic emissions that remained had their arrivals manually picked to obtain the best possible location. Any events that located outside the expected region of activity were further checked to ensure accuracy. Experience from previous studies around deposition holes showed that large source location errors were produced if significant portions of a ray path passed through the excavated deposition hole void. This only becomes a problem for the largest AEs. AEs were reprocessed with these ray paths removed.

6. Finally, a filter was applied to remove all AEs with a location error greater than 1.0.

During the equipment installation phase, calibration shots have been undertaken to assess the sensitivity of the system to 'real' AEs and to determine the accuracy with which real events could be subsequently located by the array of sensors. A series of test 'shots' were performed on the wall of deposition hole DA3545G01 (Figure 4-17). The shots consisted of undertaking 10 'pencil lead breaks' and 10 hits with a screw-driver at 1 metre intervals down 4 lines along the deposition hole wall. The pencil-lead tests involved breaking the 0.5 mm lead from a mechanical pencil against the borehole wall. This is a 'standard' analogue for an AE as it generates a similar amount of high-frequency energy. An example of a pencil lead break test is shown in Figure 4-18. This was made at 6 metres below the tunnel surface on the deposition hole wall at a point adjacent to borehole KA3548G02. This corresponds to an AE source dimension on the millimetre scale (grain size).

The screw-driver hits provided a good amplitude signal for assessing the accuracy with which events can be located within the volume surrounded by the array. Figure 4-17 shows the results from one processed set of locations for a line of shots down the deposition hole wall. This shows that the array is able to locate events with good accuracy and consistency within an estimated uncertainty of approximately 10cm.
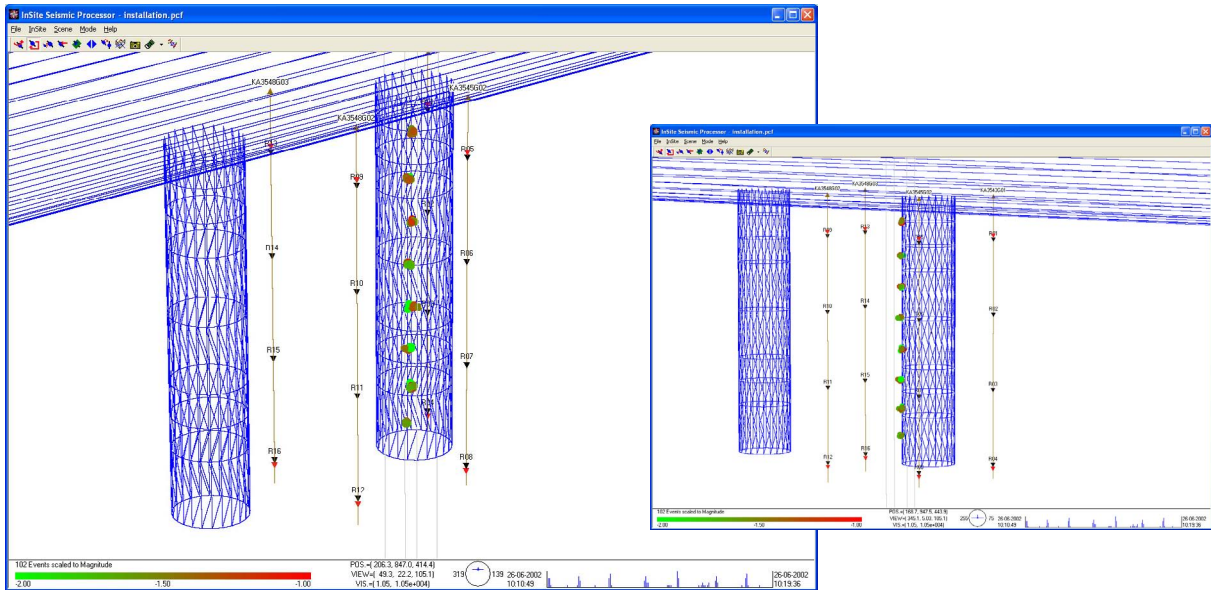
Figure 4-17. *Locations of calibration shots obtained from a series of tests at 1 metre intervals down the wall of deposition hole DA3545G01. The two views show that these line up and are located close to the surface of the hole.*
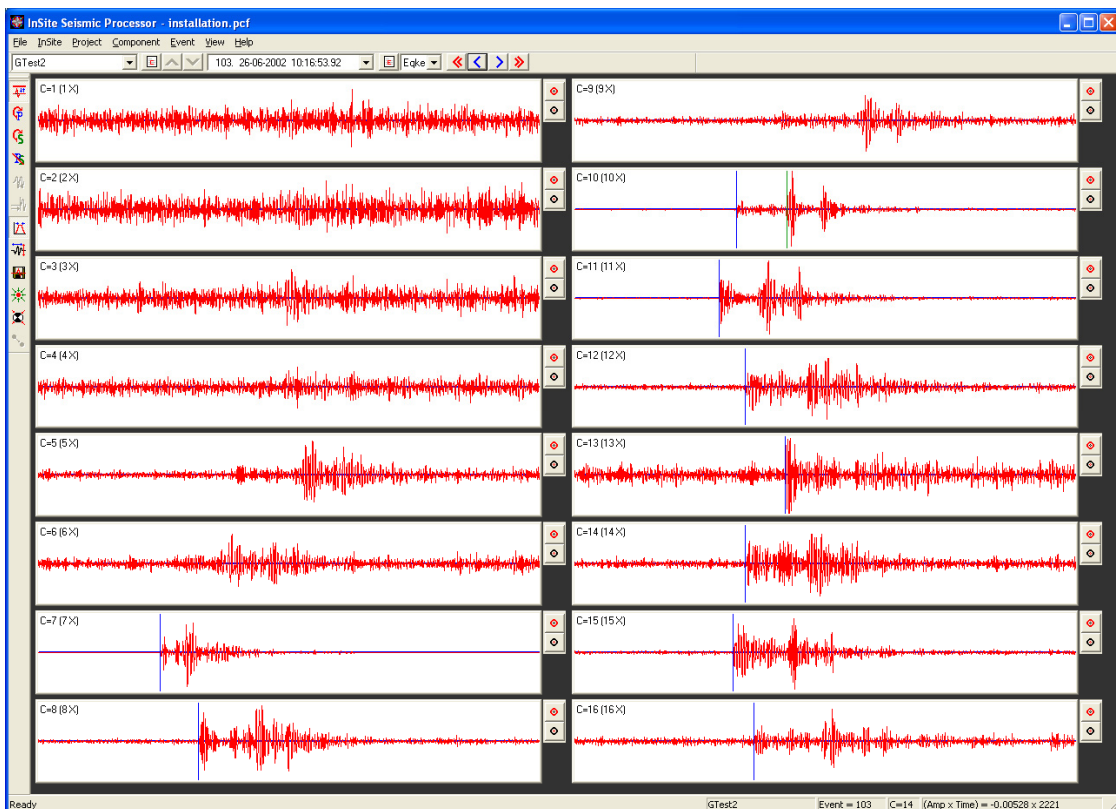
Figure 4-18: *Example waveforms from each of the 16 receiving channels for a 'pencil-lead break' test undertaken against the Deposition Hole (DA3545G01) wall 6 metres below the tunnel floor.*

Appendix III   Processing Parameters

A: Ultrasonic survey processing parameters:

PROCCESSING PARAMETERS   **Velocity survey processing**

EVENT INITIALISATION	
View/process waveforms by	Channel
Channel-view Width-to-height ratio	6
Waveform Response type	Set from sensor
Sampling time	1
Time units	Microseconds
Pre-signal points	200
Spline sampling time	0.2
Waveform To point	1023
P-Time correction	0
S-Time correction	0
Automatically update Channel Settings	NOT SET
Project Files	NULL

AUTO PICKING	
Allow P-wave-autopicking	YES, Use first peak in the auto-pick function
Back-window length	100
Front-window length	35
Picking Threshold	4
Min. Peak-to-Peak amplitude	0
Allow S-Wave Autopicking	YES, Use first peak in the auto-pick function
Back-window length	100
Front-window length	35
Picking Threshold	3
Min. Peak-to-Peak amplitude	0
Allow Automatic Amplitude Picking	YES
Use Velocity Window Picking	YES
P-wave Min. Velocity/Max. Velocity	4500, 6500
S-wave Min. Velocity/Max. Velocity	2500, 3500

CROSS-CORRELATION	
CCR Events	Referenced to a Survey
Reference Component	20041208005920
Reference Event	NULL
Window construction method	Front to Back
Window comparison method	Fixed to reference picks
Window Parameters	Back-window length = 20
	Front-window length=30
	Rise-time multiplier = NULL
	Power to raise waveform =1
	Split to a Spline function = YES
	Obtain absolute waveform= NOT SET

LOCATER	*(not used in velocity surveys)*
Method	SIMPLEX INTO GEIGER
Method settings	Tolerance = 0.01
Simplex settings	LPNorm = 1
	P-wave weighting = 1
	S-wave weighting = 1
	Use Outlier Identification = NOT SET
	Arrival error factor = ×2
Geiger settings	Tolerance (Loc. units) = 0.01
	Step size (Loc.units) = 0.1
	Max. Iterations = 100
	Conditional No. Limit = 10000000000
Velocity Structure	Homogeneous Isotropic
Velocity Structure settings	P-wave velocity = 6000 m.s^{-1}
	S-wave velocity = 3350 m.s^{-1}
	Attenuation = 200
	Q(S) value = 100
Data to use	P-wave Arrivals Only
Distance units	Metres
Working time units	Microseconds
Min P-wave arrivals	0
Min S-wave arrivals	0
Min Independent arrivals	5
Max. Residual	20
Start point	Start at the centroid of the array
Write report to RPT	NOT SET
Source parameters	Set to calculate automatically

B: AE processing parameters:

PROCCESSING PARAMETERS   **AE processing**

EVENT INITIALISATION	
View/process waveforms by	Channel
Channel-view Width-to-height ratio	6
Waveform Response type	Set from sensor
Sampling time	1
Time units	Microseconds
Pre-signal points	200
Spline sampling time	0.2
Waveform To point	1023
P-Time correction	0
S-Time correction	0
Automatically update Channel Settings	SET
Project Files	NULL

AUTO PICKING	
Allow P-wave-autopicking	YES, Use max peak in the auto-pick function
Back-window length	100
Front-window length	35
Picking Threshold	5
Min. Peak-to-Peak amplitude	0
Allow S-Wave Autopicking	YES, Use max peak in the auto-pick function
Back-window length	100
Front-window length	35
Picking Threshold	5
Min. Peak-to-Peak amplitude	0
Allow Automatic Amplitude Picking	NOT SET
Use Velocity Window Picking	YES
P-wave Min. Velocity/Max. Velocity	4500, 6500
S-wave Min. Velocity/Max. Velocity	2500, 3500

CROSS-CORRELATION	*(not used in AE processing)*
CCR Events	NOT SET
Reference Component	NOT SET
Reference Event	NULL (not activated)
Window construction method	Individual
Window comparison method	Fixed to reference picks
Window Parameters	Back-window length = 20
	Front-window length = 30
	Rise-time multiplier = NULL
	Power to raise waveform =1
	Split to a Spline function = NOT SET
	Obtain absolute waveform= NOT SET

LOCATER	
Method	SIMPLEX INTO GEIGER
Method settings	Tolerance = 0.01
Simplex settings	LPNorm = 1
	P-wave weighting = 1
	S-wave weighting = 1
	Use Outlier Identification = NOT SET
	Arrival error factor = ×2
Geiger settings	Tolerance (Loc. units) = 0.01
	Step size (Loc.units) = 0.1
	Max. Iterations = 100
	Conditional No. Limit = 10000000000
Velocity Structure	Homogeneous Isotropic
Velocity Structure settings	P-wave velocity = 5986.106 m.s^{-1}
	S-wave velocity = 3349.171 m.s^{-1}
	Attenuation = 200
	Q(S) value = 100
Data to use	P-wave Arrivals Only
Distance units	Metres
Working time units	Microseconds
Min P-wave arrivals	0
Min S-wave arrivals	0
Min Independent arrivals	5
Max. Residual	20
Start point	Start at the centroid of the array
Write report to RPT	NOT SET
Source parameters	Set to calculate automatically

EVENT FILTER	
Date and Time	NOT SET
Location volume	Minimum = (235, 880, 420)
	Maximum = (300, 964, 463)
L. Magnitude	NOT SET
Location Error	1
Independent Instruments	Minimum = 0

SOURCE PARAMETERS	
Automatic source-parameter windows	P-wave back window = 10
	P-wave front window = 50
	S-wave back window = 10
	S-wave front window = 50
Source parameter calculations	Min number to use = 3
Automatic source-parameter windows	Apply Q correction = SET
	Source density = 2640
	Source shear modulus = 39131400000
	Av. radiation coefficient: Fp = 0.52 ,Fs = 0.63
Source parameter calculations	Source coefficient: kp = 2.01 , ks = 1.32
Magnitude calculations	Instrument magnitude = 1 * log (ppV) +0
	Moment magnitude = 0.666667 * log(Mo) + -6